Powder Technology 286 (2015) 488–506

Contents lists available at ScienceDirect

Powder Technology

journal homepage: www.elsevier.com/locate/powtec

# CFD simulation of cyclone separators to reduce air pollution

Sakura Ganegama Bogodage *, Andrew Y.T. Leung

*Department of Architectural and Civil Engineering, City University of Hong Kong, 83 Tat Chee Avenue, Kowloon, Hong Kong SAR, China*

ARTICLE INFO

Available online 5 September 2015

*Keywords:*
Cyclone separator
Computational fluid dynamics
Down-comer tube
Large Eddy Simulation
Solid loading rate

ABSTRACT

The present paper is based on CFD modelling of gas–solid flow in cyclone separators with different dust outlet geometries (with and without down-comer tubes at the cyclone bottom) to analyse the flow characteristics and the cyclone performance. Numerically obtained cyclone performance parameters, collection efficiency, and pressure drop were compared with experimental results. Changes in the particle trajectories due to the variation of the flow field inside the cyclone separators with the effect of the dust outlet section were also analysed in detail. The simulation results largely agreed with the experimental results, and discrepancies were caused by modelling limitations and inconsistencies of the particle tracking model with the real gas–solid flow. However, comparable to the experiments, the CFD simulations also predicted the increments in collection efficiencies by dust outlet geometries modified with down-comers within acceptable pressure drops.



## 1. Introduction

Application of cyclone separators in particle controlling industries (e.g., air pollution control, aerosol sampling and particulate matter control [1]) is an economical method for efficiently removing particles larger than 2 μm in size [2]. The particle separation inside cyclone separators manages two swirling motions of the fluid flow in vertically opposed directions (double vortex phenomenon). Centrifugal forces acquired in the particles due to these swirling motions directly separate larger particles, but small particles depart with the flow. However, because of the vortex phenomenon, the conical section and the dust collection section are very important in particle separation although they have been neglected in many studies.

Studies related to the geometric parameters of the cone (height and bottom opening) are popular in the literature, but few studies have considered the cyclone performance comparing the particle collection section. In practical applications, the geometry of this part has also not been considered yet nor have the use of different types of geometries and connections with the space availability. Bryant et al. [3] (as quoted by Xiang et al. [4]), Zhu and Lee [5] and Mothes [6] (as reported by Obermair et al. [7]) reported that the solid separation at the cyclone bottom is important in collection efficiency due to the effects from the natural vortex length of the flow, higher tangential velocities, particle re-entrainment and high particle concentrated zones.

With the geometric limitations of the cyclone cone and apex size due to the natural vortex length of the cyclones, considerations passed to the geometry of the dust collection section to enhance the cyclone performance. Research based on the dust collection geometry of cyclone separators to minimize the solid re-entrainment from this section were tested considering apex cones, additional hoppers and down-comer tubes [7–9]. Obermair and Staudinger [8] showed the superiority of down-comer tubes in increasing cyclone performance over other modifications. The best collection efficiency was achieved by the cyclone separator modified by a down-comer that is half of the cyclone height.

As stated by Obermair et al. [7], down-comer tubes have been introduced by Kecke [10] without any experimental investigations on enhancing collection efficiency from the dust collection section. Later, Obermair et al. [7] and Hoffmann et al. [9] proved remarkable improvements in the collection efficiency by extending the natural vortex length further, thus reducing the particle re-entrainment. The study performed by Gil et al. [11] using only a down-comer tube without a hopper resulted a higher separation efficiency of small particles (for 0 to 5 μm more than 87 %) while producing "fishhook-shaped" fractional efficiency curves. This study was conducted at relatively higher solid loading rates (85.2 to 202.8 g/m$^3$), where the particle agglomeration and spontaneous separation dominate at the inlet. The downward penetration of the vortex end was reduced with increasing solid loading [9], which raised the requirements for more investigations of down-comer designs.

Over the last decade, CFD simulations have been promoted in fluid mechanics as a design tool, providing better results while minimizing time and cost compared to experimental investigations. Identical to the experimental results of Obermair and Staudinger [8], CFD studies completed by Hoffmann et al. [12], Qian et al. [13] and Kaya and Karagoz [14] showed significant particle removal capability of down-comers and their optimal length, which approximately equals the half-height of the cyclone separator. Qian et al. [13] and Kaya and Karagoz [14] also showed less effect on pressure drops in the application of down-

* Corresponding author.
*E-mail addresses:* sganegama2-c@student.cityu.edu.hk, sakurabogoda@gmail.com (S. Ganegama Bogodage).

http://dx.doi.org/10.1016/j.powtec.2015.08.023
0032-5910/

comer vertical tubes, which could be explained by the decrease of wall friction due to reduction of particle re-entrainment from the hopper into the cyclone.

However, a comprehensive analysis of performance including flow characteristics and particle trajectories has not yet been conducted for cyclone separators with down-comers. Therefore, the present study is based on the numerical analysis of cyclone separators modified with down-comer tubes compared to experimental investigations.

Experimental studies were conducted for identical geometric and operational conditions, and the overall collection efficiencies were calculated by weighing the collected particle mass inside the cyclone body. The grade efficiencies were obtained by counting the particle fractions in iso-kinematic flow samples using a Fluke particle counter (Fluke 983, FLUKE Inc.) from the inlet and outlet. Measurements of pressure drop were obtained using Air Flow Meter (TSI PVM620), considering the mean pressure difference between the inlet and the outlet.

## 2. Numerical simulation

### 2.1. Geometric parameters of the cyclone separator and down-comer tubes

The geometric parameters of the cyclone separator tested in this study are given in Fig. 1 and Table 1. Two conventional dust outlets and three dust outlets modified with down-comer tubes were considered for the simulations. The dimensions of the dust outlet geometries are shown in Table 2.

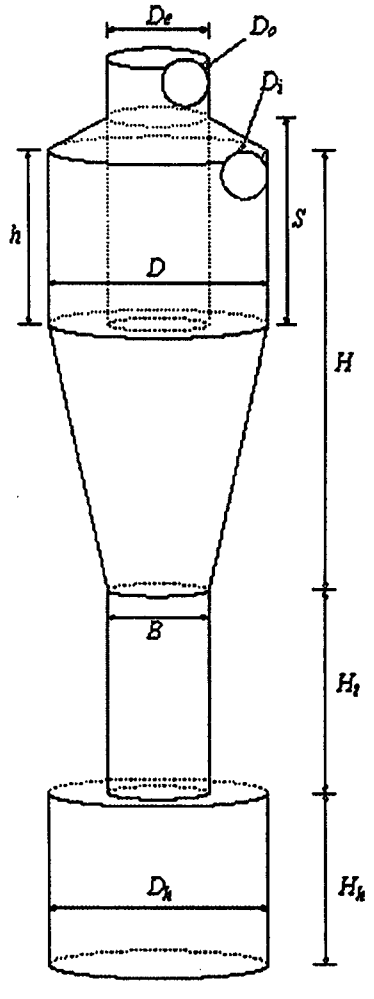


Fig. 1. Geometry of the cyclone separator.

Table 1
Geometric properties of cyclone separator.

| Geometric parameter | Dimension (mm) |
|---|---|
| Body diameter, $D$ | 330.200 |
| Inlet/Outlet pipe diameters, $D_i/D_o$ | 69.120 |
| Cyclone cylindrical body height, $h$ | 254.000 |
| Cyclone conical body height | 390.525 |
| Cyclone total height, $H$ | 693.7375 |
| Vortex finder height, $S$ | 303.2125 |
| Vortex finder diameter, $D_e$ | 152.400 |
| Cone tip diameter, $B$ | 152.400 |
| Hopper height, $H_h$ | 254.000 |

### 2.2. Numerical procedure

#### 2.2.1. Computation of the grid

Geometry and meshing were developed by ANSYS CFX software. Tetra meshing was used due to the geometric complexity, as recommended by CFX for Large Eddy Simulation (LES) model [15]. The number of elements in each meshed geometry is shown in Table 3.

#### 2.2.2. Model setup

Simulations were performed in ANSYS CFX 14.0. ANSYS CFX solver is an implicitly coupled solver that uses element-based finite volume methods to discretize the governing equations in the spatial domain [16]. CFX uses the Rhie and Chow [17] pressure–velocity coupling method on a co-located grid layout. The simulations were conducted in a Blade Centre H Linux cluster in MPICH distributed parallel mode.

#### 2.2.3. Boundary conditions

Setting boundary conditions in numerical modelling is simply defining the properties at domain surfaces that help to fully describe the flow characteristics. Air at 25 °C was used as the continuous phase and particles (size range 0–18 μm; density 2650 kg/m$^3$) were specified as particle transport solids (dispersed phase). Atmospheric pressure was used as the reference pressure. The boundary conditions applied in the simulations are given in Table 4.

In Table 4, attention was given to defining the particle collection surface. In reality, particles are deposited on cyclone walls just after entering, and the rest are suspended in the flow and separated by the centrifugal action accomplished with particle agglomeration, while some may leave without collecting. However, this reality is difficult to model in CFD, as there is no evidence on whether, when or where a particle is collected.

Particles that touched the cyclone hopper bottom were counted as collected by Kepa [18], Wan et al. [19] and Qiu et al. [20]. Ma et al. [21] assumed that particles that touched the cyclone wall were collected, while Griffiths et al. [22] considered particles that touched the conical part and the bottom walls to be collected. The assumption based on studies by Yoshida et al. [23], Gimbun et al. [24], Chuah et al. [25] and Bhaskar et al. [26] was that the particles that escaped from the cyclone bottom were collected. The number and mass of particles that escaped from the cyclone during the simulation period are also considered as collected in the literature [27–29]. In summary, the conclusions derived

Table 2
Dimensions of dust outlet geometry.

| Dust outlet condition | Height of down comer tube, ($H_t$, mm) | Diameter of dust collection hopper ($D_h$, m) |
|---|---|---|
| Hopper 1 | 0.0 | 152.4 |
| Hopper 2 | 0.0 | 288.0 |
| Hopper 3 | 127.0 | 288.0 |
| Hopper 4 | 254.0 | 288.0 |
| Hopper 5 | 381.0 | 288.0 |

**Table 3**
Total number of elements in the mesh.

| Geometric condition | Number of elements |
|---|---|
| Hopper 1 | 1,158,227 |
| Hopper 2 | 1,348,628 |
| Hopper 3 | 1,377,011 |
| Hopper 4 | 1,427,762 |
| Hopper 5 | 1,505,334 |

for the selection of particle deposition zones in cyclone separators in CFD simulations are unclear.

A numerical study by Shi and Bayless [30] studied three different particle boundary conditions: 1) assume that particles were only collected by the bottom of the cyclone, 2) assume that particles were collected by the wall of the cone and the bottom and 3) apply the tangential lift-off boundary condition to the wall of the cone and the bottom. The numerical results were compared to the experimental results of Bohnet [31], Lim et al. [32] and Yoshida et al. [33], and the boundary condition that applied the tangential lift-off boundary condition to the wall of the cone and the bottom was much closer to the real state results. The assumption that the particles were collected by the wall of the cone and the bottom always over predicted the results. However, the boundary condition assuming that particles were only collected by the bottom of the cyclone was also acceptable. Another study by De Souza et al. [34] considered two particle collection criteria: 1) particles escaped from the outlet and 2) particles touched the cone bottom. The second criterion is reasonable with the experimental results but can over predict fine particle collection as there is no re-entrainment from the cone bottom. However, the authors found that the grade efficiency curves do not converge after the cyclone residence time, and thus particles may bounce back and escape from the outlet, leading to an under prediction of collection efficiencies assuming particles escaping from the outlet. Therefore, assuming particles that touched the hopper bottom were assumed to be collected in this study.

### 2.2.4. Modelling fluid flow

The Large Eddy Simulation (LES) model preserves accurate predictions of unsteady, spiral shape, and vortex core characteristics of a cyclone separator [35–43]. This model resolves larger energy carrying eddies, while smaller energy eddies are filtered to be simulated by sub-grid scale (SGS) models rather than simulating the entire turbulence flux [44]. The present study applied a finite volume based LES model to simulate the gas–solid flow inside cyclone separators, accomplished with the Smagorinsky–Lilly SGS model.

*2.2.4.1. LES governing equations.* Considering resolved and sub-grid components, any variable ($\varphi_i$) can be written as a combination of the resolvable scale part ($\overline{\varphi}_i$) and the subgrid-scale part ($\varphi'_i$),

$$\varphi_i = \overline{\varphi}_i + \varphi'_i . \tag{1}$$

Then the basic filtered variable ($\overline{\varphi}_i$) is defined in spatial coordinates ($x$, $\xi$) in considered domain;

$$\overline{\varphi}_i(x,\ t) = \int G(x-\xi)\varphi(\xi,\ t)d\xi. \tag{2}$$

The incompressible Navier–Stokes equation of motion is shown in Eq. (3).

$$\frac{\partial \rho v_i}{\partial t} + \frac{\partial \rho v_i v_j}{\partial x_j} = -\frac{\partial p}{\partial x_i} + \frac{\partial}{\partial x_j}\left[\mu\left(\frac{\partial v_i}{\partial x_j} + \frac{\partial v_j}{\partial x_i}\right)\right]. \tag{3}$$

Then average and time varying components in both variables velocity ($u_i$) and pressure ($p$) can be written as in Eq. (4),

$$v_i = \overline{v}_i + v'_i,\ \ p = \overline{p} + p'. \tag{4}$$

By substituting Eq. (4) in to Eq. (3), the filtered Navier–Stokes equation is given by:

$$\frac{\partial \rho \overline{v}_i}{\partial t} + \frac{\partial \rho \overline{v_j}\ \overline{v_i}}{\partial x_j} = -\frac{\partial \overline{p}}{\partial x_i} + \frac{\partial}{\partial x_j}\left(\mu\frac{\partial \overline{v}_i}{\partial x_j} + \frac{\partial \overline{v}_j}{\partial x_i}\right) - \frac{\partial \tau_{ij}}{\partial x_j}. \tag{5}$$

Here the extra term $\partial\tau_{ij}$ represents subgrid-scale stresses and hence can be represented by,

$$\tau_{ij} = \overline{v_i v_j} - \overline{v}_i \overline{v}_j \tag{6}$$

where,

$$v_j \frac{\overline{\partial v_i}}{\partial x_j} \neq \overline{v}_j \frac{\partial \overline{v}_i}{\partial x_j}. \tag{7}$$

*2.2.4.2. Smagorinsky model equations.* The Smagorinsky–Lilly SGS model is the first SGS model developed by Smagorinsky [45] and assumes that the energy production and dissipation of the small scales are in equilibrium.

The Smagorinsky model expressed sub-grid scale stresses ($\tau_{ij}$) as,

$$\tau_{ij} - \frac{1}{3}\tau_{kk}\delta_{ij} = -2\nu_{SGS}\overline{S}_{ij} \tag{8}$$

where $\overline{S}_{ij}$ is the large scale strain rate tensor defined by;

$$\overline{S}_{ij} = \frac{1}{2}\left(\frac{\partial \overline{v}_i}{\partial x_j} + \frac{\partial \overline{v}_j}{\partial x_i}\right). \tag{9}$$

The relationship between SGS turbulent viscosity ($\nu_{SGS}$) with length scale ($l$) and velocity scale ($q_{SGS}$) of sub-grid part can be expressed as,

$$\nu_{SGS} \propto l q_{SGS}. \tag{10}$$

**Table 4**
Boundary conditions of present simulation.

| Boundary | Applied boundary condition | Details |
|---|---|---|
| Inlet | Inlet | Normal speed of 10 m/s |
| Outlet | Opening | Opening and pressure drain with relative pressure of 0.0 Pa |
| Cyclone walls excluding hopper base | Wall | No-slip, smooth walls with perpendicular/parallel coefficient of restitution is 1.0. |
| Hopper base (particles contact this surface are considered as collected) | Wall | No-slip, smooth walls with perpendicular/parallel coefficient of restitution is 0.0. |
| Particle injection | Uniform injection (randomly distributed over the inlet surface) | 10000 of particle parcels having a normal speed of 10 m/s with concentration of 1.0 g/m$^3$. |

The length scale ($l$) of sub-grid part is the filter width (or grid size) and is usually taken to be,

$$\Delta = (Volume)^{\frac{1}{3}}. \tag{11}$$

In Smagorinsky model the velocity scale ($q_{SGS}$) is related to gradients of the filtered velocity as it is analogous to the Prandtl mixing length model. Then the velocity scale ($q_{SGS}$) can be written as in Eq. (12)

$$q_{SGS} = \Delta|\bar{S}| \tag{12}$$

where,

$$\bar{S} = \sqrt{2\,\bar{S}_{ij}\bar{S}_{ij}}. \tag{13}$$

Then SGS viscosity $\nu_{SGS}$ is written as,

$$\nu_{SGS} = (C_S\Delta)^2|\bar{S}|. \tag{14}$$

Here, $C_S$ is Smagorinsky constant and its value for isotropic turbulence with initial range spectrum is,

$$E(k) = C_k\,\epsilon^{2/3}k^{-5/3} \tag{15}$$

with,

$$C_S = \frac{1}{\pi}\left(\frac{2}{3C_k}\right)^{3/4} = 0.18\,. \tag{16}$$

Eqs. 1–16 are referred from ANSYS CFX 14-Solver Theory Guide [16].

The value 0.1 is used as the default value of $C_s$ and has proven the validity of results by achieving best results for a wide range of flows [16].

*2.2.5. Modelling of the particle phase*

The Eulerian–Lagrangian approach models the dispersed phase by tracking a large number of representative particles (parcels) to represent a group of particles interacting with the fluid. These representative particles have the same physical characteristics (*e.g.*, size distribution and mass) and are simulated through the previously computed continuous phase [46].

The equation of particle motion is based on the following assumptions: 1) The particles are perfectly spherical in shape, 2) The volume fraction of the dispersed phase in the continuous region is negligible, and thus no influence was due to the presence of the particles, 3) With the dilute particle flow in continuous flow, there are zero inter-particle interactions and 4) Collisions between particles and the wall are assumed to be perfectly elastic. Under these assumptions, the particle trajectories are obtained by integrating the force balance on the particle. Considering a small particle moving under the forces of nonlinear drag and gravity, the Eulerian–Lagrangian equation is given by,

$$\frac{du_{Pi}}{dt} = \frac{18\mu}{\rho_p d_p^2}\,\frac{C_D R_e}{24}\,(u_i - u_{Pi}) + g_i\left(\frac{\rho_P - \rho_g}{\rho_P}\right). \tag{17}$$

In cyclone hydrodynamics, other forces that act on the particles such as buoyancy, virtual mass and Basset term are negligible due to the small fluid-to-particle density ratio [25].

The relative Reynolds number is,

$$R_e = \frac{\rho_g d_P}{\mu}|u_{Pi} - u_P|. \tag{18}$$

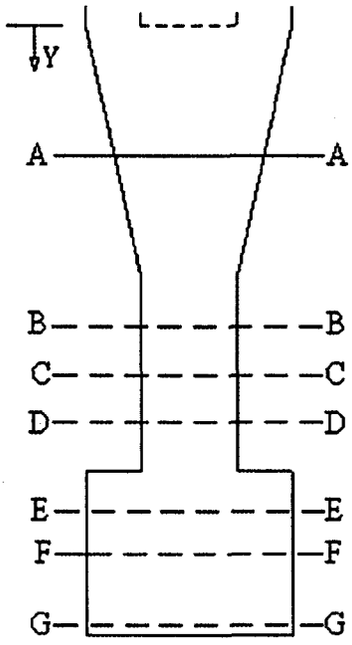


**Fig. 2.** Considered cross sections in cyclone separator body.

The drag coefficient ($C_D$) in Eq. (17) is described by the Schiller Naumann drag model as shown in Eq. (19) [16],

$$C_D = \begin{cases} \dfrac{24}{Re} & R_e \le 1 \\ \dfrac{24\left(1 + 0.15R_e^{0.687}\right)}{R_e} & 1 \le R_e \le 1000 \\ 0.44 & R_e > 1000 \end{cases} \tag{19}$$

*2.2.6. Particle coupling and drag force*

One-way coupling was selected with the negligible volume fraction of particles, extruding the influence of particle mass into fluid flow [47,48], and only the particles injected and collected are considered. The Schiller–Naumann drag model was used under the assumption of the equation of particle motion.

*2.2.7. Advection and transient schemes*

CFX strongly recommends using the Central Difference Advection Scheme [15] for LES models, combined with a Second-Order Backward Euler scheme as the transient scheme. When running the Second-Order Backward Euler scheme, the transient scheme for turbulence

**Table 5**
Details of cross sections considered in analysing.

| Section | Distance from vortex finer inlet (mm) (Measured in Y-direction) | | | | |
|---|---|---|---|---|---|
| | Hopper 1 | Hopper 2 | Hopper 3 | Hopper 4 | Hopper 5 |
| A-A (inside conical section) | 200.000 | 200.000 | 200.000 | 200.000 | 200.000 |
| B-B (down-comer tube top plane/s) | - | - | - | 454.025 | 517.525 |
| C-C (middle plane of down-comer tube) | - | - | 454.025 | 517.525 | 581.025 |
| D-D (down-comer tube bottom plane) | - | - | 503.000 | 630.000 | 757.000 |
| E-E (top plane of hopper) | 454.025 | 454.025 | - | - | - |
| F-F (Middle plane of hopper) | 517.525 | 517.525 | 644.525 | 771.525 | 898.525 |
| G-G (bottom plane of hopper) | 630.000 | 630.000 | 757.000 | 884.000 | 1.010 |

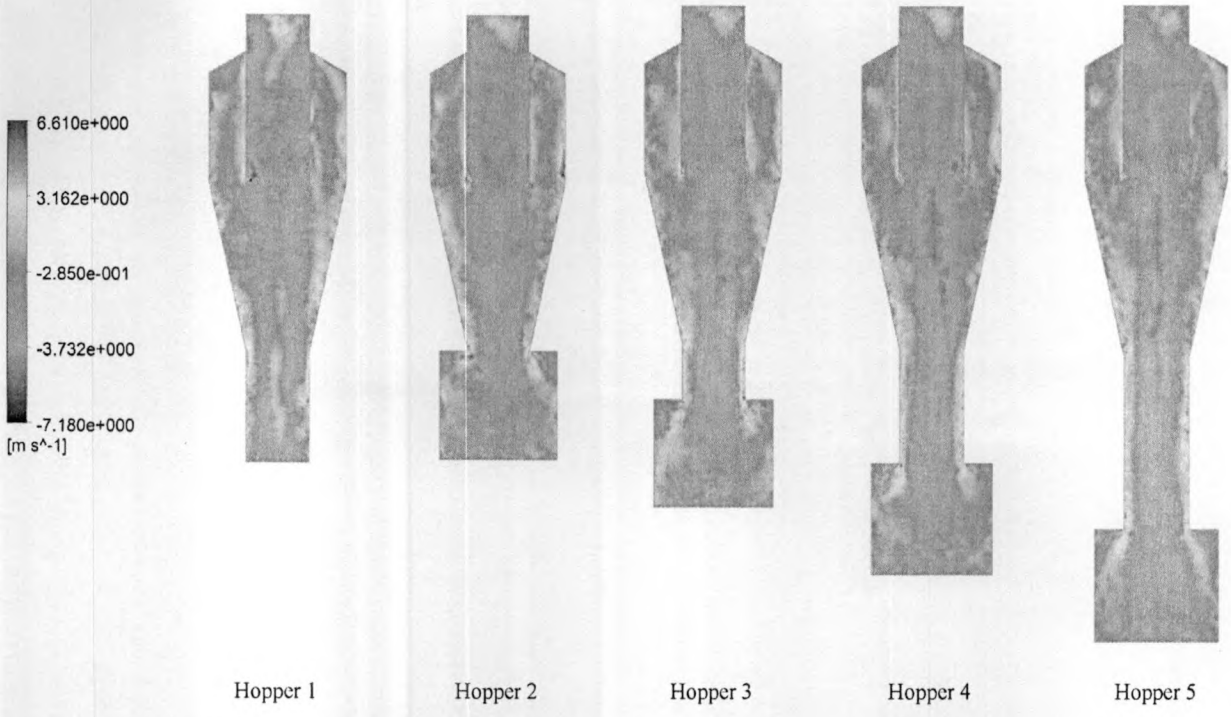


**Fig. 3.** Axial velocity contours along the vertical axis of cyclone separators with different dust outlet geometries.

equations would remain First-Order, and the transient scheme for the volume fraction equations should be set to a bounded second-order scheme [15].

*2.2.8. Convergence control*

Convergence control terminates a solver run within a time step, when it reaches the Maximum Coefficient Iteration loops, unless convergence is achieved sooner for transient state. The Minimum Coefficient Iteration loop is also defined to control the number of iterations for a time step. A model should aim to converge each time step within approximately 3–5 loops. However, in transient runs, if convergence is not achieved in the maximum number of loops, it is more preferable to reduce the time step size than to increase the number of loops [15]. In the present study, default values of iteration loops were selected and convergence was achieved within this range.

*2.2.9. Convergence criteria*

The convergence criterion is important to ensure that the governing equations have been solved. This criterion decides when the solution has converged and consequently when the solver should stop, with or without completing the maximum number of iterations. The measurement of convergence criteria is performed by residuals, which measure how accurately the set of equations have been solved. The CFX-Solver will terminate the time step when the equation residuals fall below the residual target value. The selection of the residual target depends on the sensitivity of the problem. For the present model to obtain better

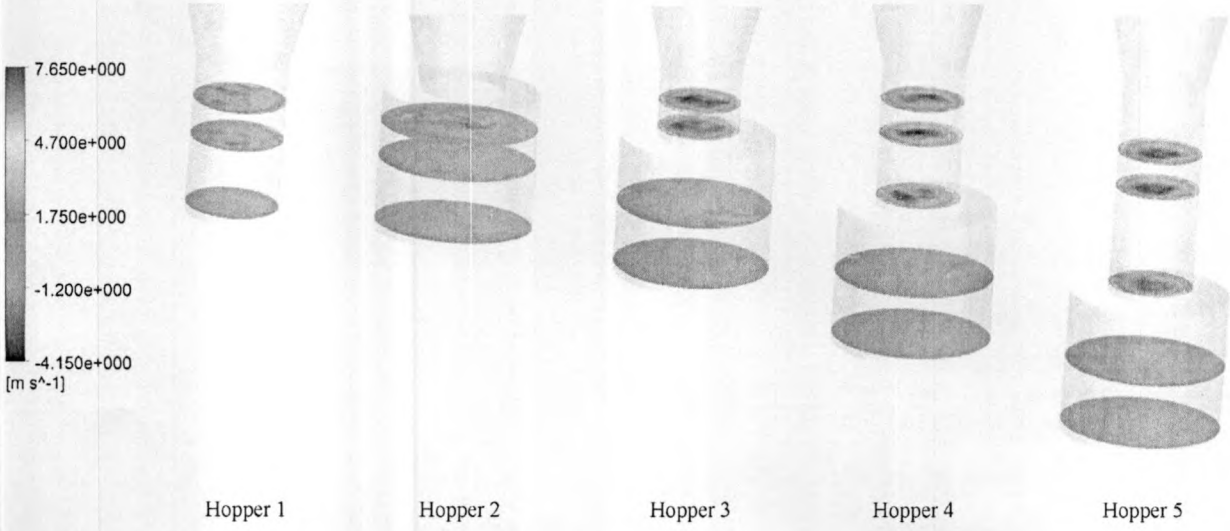


**Fig. 4.** Axial velocity contours on radial planes of different dust outlet geometries in cyclone separator.

numerical results, convergence criteria were selected as RMS residual type having a target of 1E-5.

*2.2.10. Flow analysis details*

To perform the transient run in CFX-Pre, the steady state simulation results after 100 iterations were used as initial conditions in each geometric condition. The simulations were continued until none of the particle tracking diagnostics run in the solver. Adaptive time steps were used to change the time step size dynamically within the provided time limits (the initial and maximum time steps were $1.0 \times 10^{-5}$ s and $1.0 \times 10^{-3}$ s, respectively). The total simulation time was 13 s for Hopper 1, Hopper 2, Hopper 3 and Hopper 4 and was 14 s for Hopper 5. The maximum time step in all cases achieved by the solver was $5.4 \times 10^{-5}$ s after the time of $1.0 \times 10^{-2}$ s in Hopper 1 and $7.0 \times 10^{-3}$ s in other hopper conditions. When the simulation converged, the maximum time step was used as a constant time step.

## 3. Results and discussion

The CFD simulation of the cyclone separator flow field was analysed considering three velocity components (axial, tangential and radial) and pressure variations along the cyclone body. These flow properties were analysed in the axial and planer views of the contour plots and the radial distributions along different cross sections. Fig. 2 shows the considered cross sections, and the details are listed in Table 5.

The particle trajectories were also analysed to have a basic understanding of particle flow and collection in cyclone separators. The numerical results of the collection efficiency and pressure drops were compared to the experimental data to validate the simulation results.

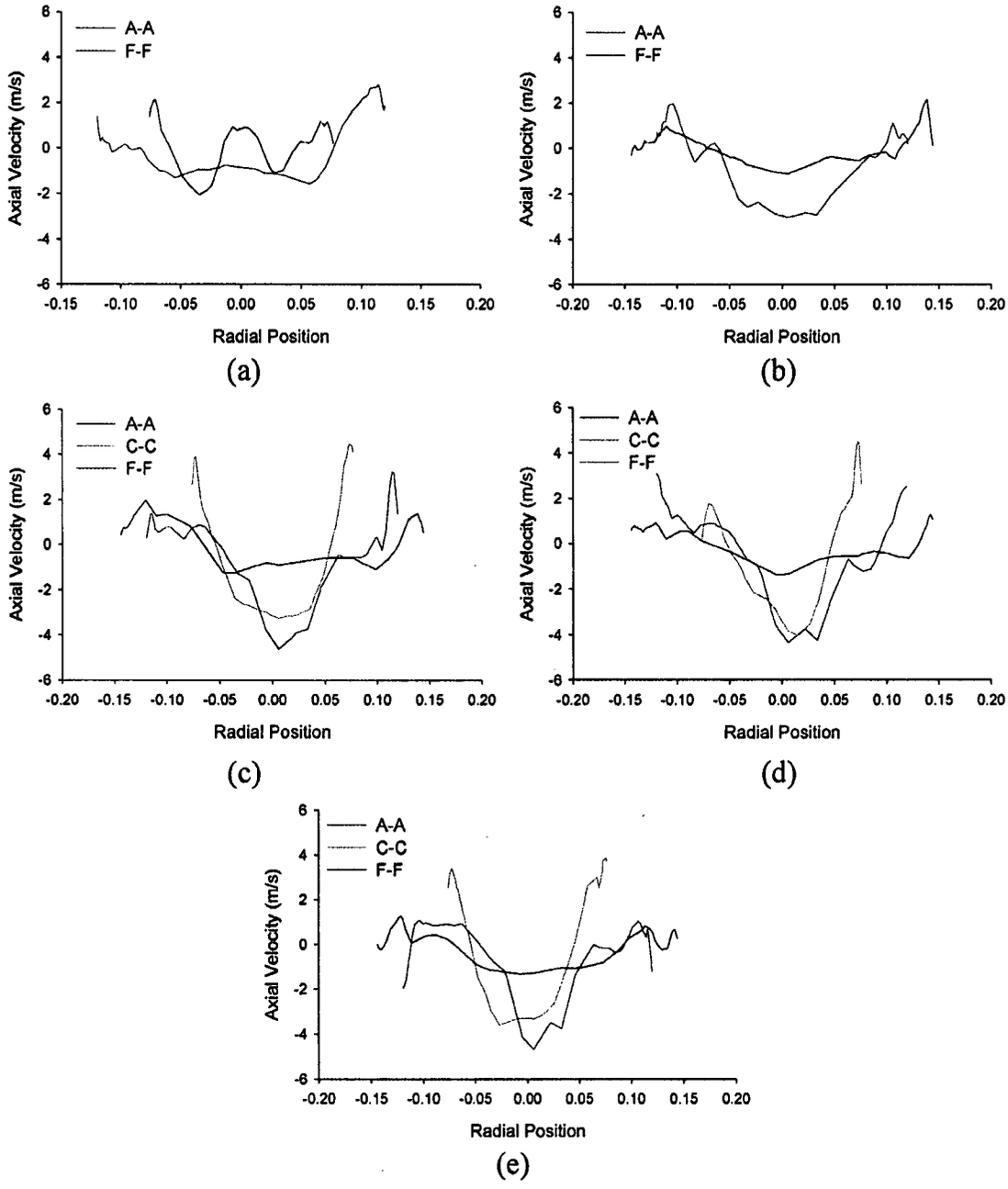


Fig. 5. Axial velocity components along radial direction at different cross sections in cyclone separator and dust outlet geometry (a) Hopper 1; (b) Hopper 2; (c) Hopper 3; (d) Hopper 4 and (e) Hopper 5.

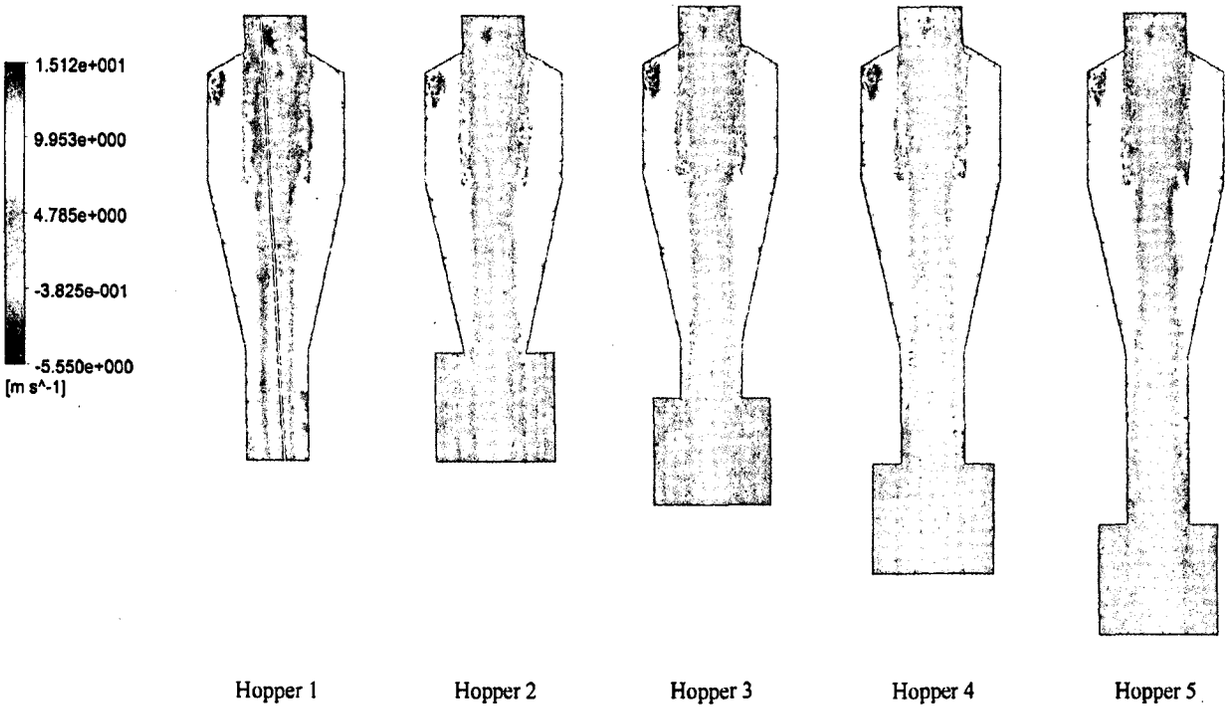


**Fig. 6.** Tangential velocity contours along the vertical axis of cyclone separators with different dust outlet geometries.

### 3.1. Flow field analysis

Among the three velocity components in the cyclone swirling flow, the tangential velocity component is the largest, which governs the swirling flow pattern and separates particles by the centrifugal forces. The axial flow is also important for transporting the collected particles on the walls to the hopper. In cyclone hydrodynamics, the magnitude of the radial velocity is negligible [49], although it contributes to transporting particles on to the walls with the effect of the centrifugal forces.

#### 3.1.1. Axial velocity

The axial velocity contours in the mid-axial plane of each hopper condition are shown in Fig. 3 (downward is positive and upward is negative). The axial velocity component is not axi-symmetric and is downwardly directed at the outer core (quasi-free vortex), which is higher near the wall region and upwardly directed in the inner core region (quasi-forced vortex). The maximum downward and upward velocities are always smaller than the inlet velocity. Conversely to this observation, earlier studies reported that the maximum axial velocity is higher than the inlet velocity, especially under the vortex finder inlet [13,50].

The axial velocity patterns with respect to the dust outlet geometries in Fig. 4 show the major difference in the forced vortex. In Hopper 1, different from the others, the axial velocity at the inner core transports back to the hopper due to flow recirculation. The maximum upward axial velocities are presented down to the vortex finder inlet, and this region extends farther down with the down-comer height. This increase of axial velocity in the leaving flow is important for increasing the collection efficiency without mixing the free and forced vortexes together in the cyclone body, mostly at low velocity or higher solid loading conditions. Inside down-comer tubes, the axial velocity is higher than inside the cyclone body and no recirculation zones, which improves collection efficiency by minimizing particle re-entrainment. However,

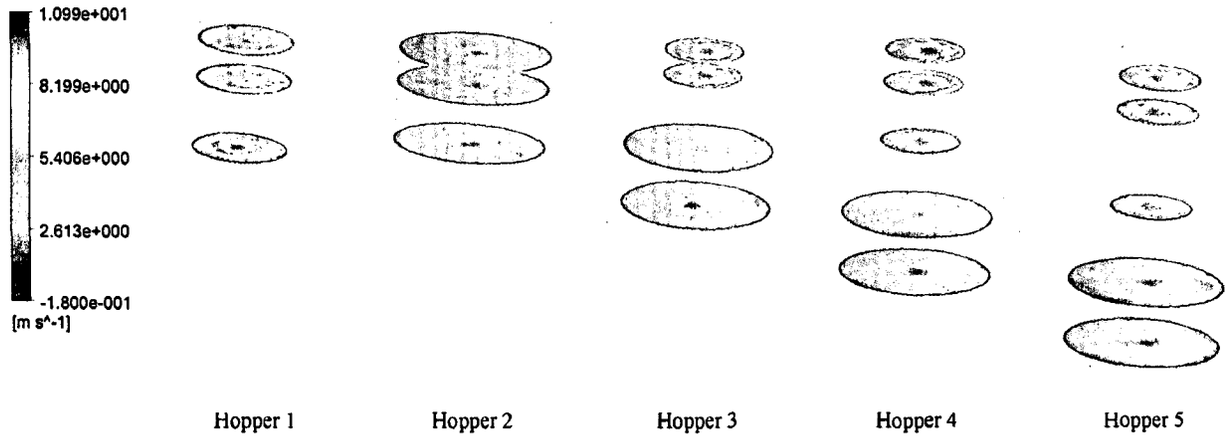


**Fig. 7.** Tangential velocity contours on radial planes of different dust outlet geometries in cyclone separator.

as shown in Fig. 4, there is no clear distribution of the axial velocity component with the effect of recirculation inside hoppers.

The axial velocity profiles of the selected cross sections from Table 5 are shown in Fig. 5. The axial velocity profiles exhibit V-shape or W-shape [51] patterns with the effect of cyclone geometry [52]. In the present study, W-shaped axial velocity pattern are more likely in the cyclone body (section A-A in Fig. 5) except in Hopper 2, but the attenuation on swirling flow by friction losses on the vortex finder walls is lowered. Thus, less swirled flows are drawn back to the cyclone body [28].

The axial velocity profiles in the radial direction are roughly V-shaped but are flatted in Hopper 2. Similar patterns were reported by Elsayed and Lacor [28] for an identical geometry. The authors also discussed the different flow patterns with the effect of dust outlet geometric conditions by considering adverse pressure gradients at the centre axis, as stated by Hoffmann et al. [12]. That is, in Hopper 2, where the diameter is approximate to the cyclone body diameter, the adverse pressure gradient due to the swirl attenuation in the vortex finder can be overcome with the higher kinetic energy resulting from the sudden contraction of the upward flow at the cone tip and obtaining V-shaped axial velocity profiles. However, in Hopper 1, the diameter is similar to the cone tip diameter, and thus it is impossible to overcome the swirl attenuation in the flow field.

However, with down-comer tubes, the effect of swirl attenuation of vortex finer friction losses could not be overcome due to less kinetic energy near the cone tip. The radial profiles at the cyclone conical region (section A-A) and in the down-comer tubes (section C-C) have similar average patterns. Comparing the axial velocities in the hoppers, Hopper 1 shows the W-pattern with the effect of backflow in a quasi-forced vortex, but the others have almost similar and insignificant features.

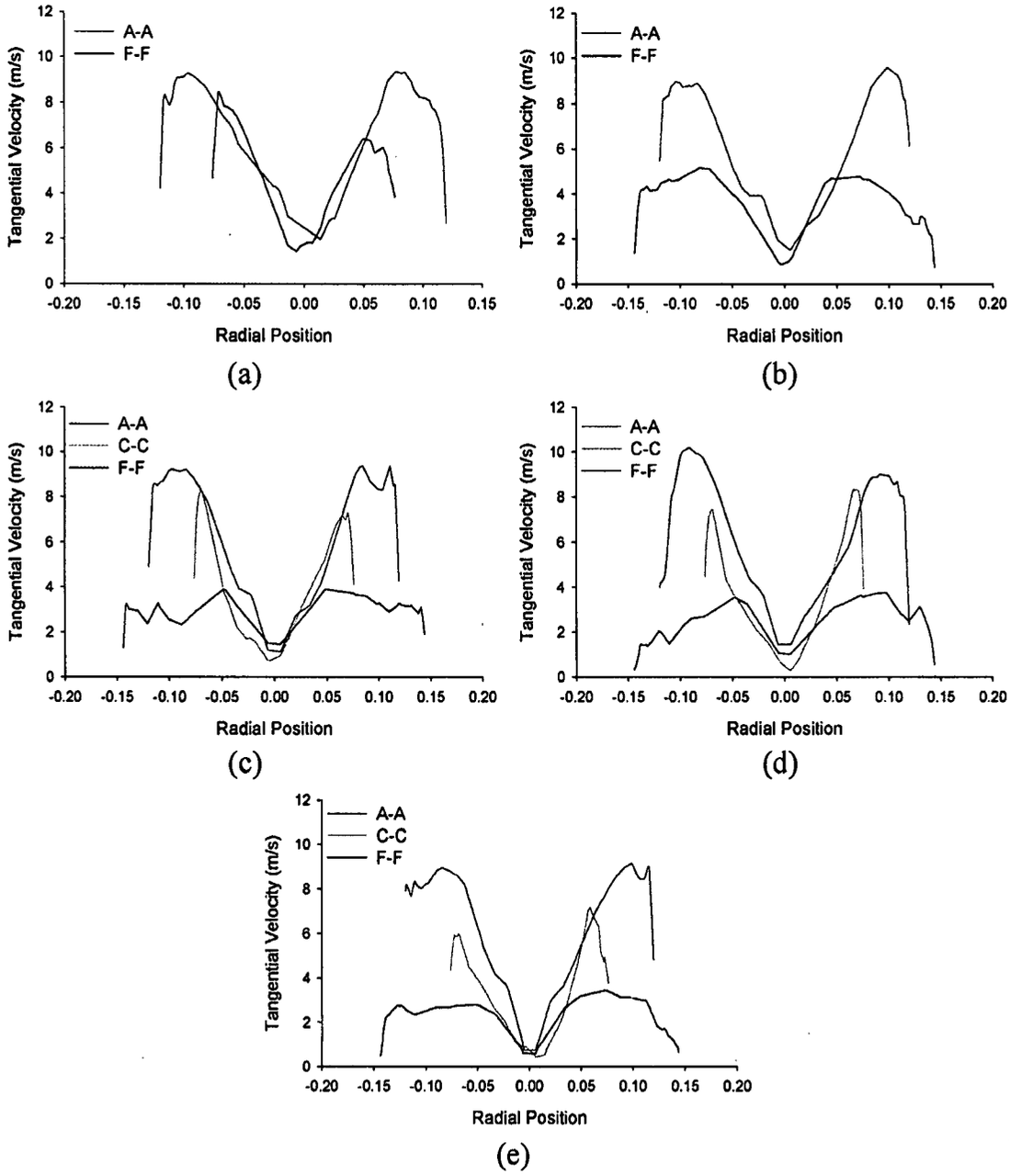


Fig. 8. Tangential velocity components along radial direction at different cross sections in cyclone separator and dust outlet geometry (a) Hopper 1; (b) Hopper 2; (c) Hopper 3; (d) Hopper 4 and (e) Hopper 5.

*3.1.2. Tangential velocity*

The tangential velocity contours at the middle plane of the cyclone separator for five different dust outlet geometries are shown in Fig. 6, and at major separation, the space tangential velocity is identical in five geometric conditions. This velocity component is the largest velocity component and dominates the swirling flow pattern, confirmed by showing a similar contour pattern with dynamic pressure (see Fig. 11). The highest tangential velocity occurred at the cyclone top. At the inlet annulus, the tangential velocity increased up to 1.5 times the inlet velocity and then decreased due to the downward rotation of the flow. Negative tangential velocities are found at the cyclone gas outlet because the moving direction of flow is opposite to the inlet flow.

The tangential velocity exhibits Rankine double vortex phenomenon with quasi-free vortex at the outer core, where the tangential velocity sharply increases with increasing radius and reaches a maximum value closer to the vortex finder diameter. In a quasi-forced vortex in the inner core, the tangential velocity decreases further to nearly zero at the axis centre. The maximum tangential velocity in the cyclone inner region (bottom to cyclone inlet) is almost similar to the inlet velocity, and similar observations are reported by Elsayed and Lacor [27] for three types of cyclone separators with different cone tip diameters at an inlet velocity of 8 m/s. The maximum tangential velocity is located at approximately 0.8 to 1.0 of the radius of the vortex finder from the cyclone centre axis, agreeing with former research that showed 0.5 to 0.9 times [27] the vortex finer radius.

Considering the conventional designs (Hopper 1 and Hopper 2) shown in Fig. 7, the tangential velocity was not reduced inside the hoppers and was higher in Hopper 1, thus possibly worsening the collection efficiency. However, with down-comers at the bottom of the cyclone, the tangential velocity falls inside the hopper and the reduction is greater with down-comer height. Inside the down-comer tubes, the tangential velocity is dramatically increased in quasi-free vortex flow as a result of reducing the cross section, but the flow is reduced axially towards the hoppers. In the quasi-forced vortex region in the hoppers, the reduction of tangential velocity is identical to the quasi-forced vortex region in the cyclone body comparing the minimum values of sections A-A and F-F. However, the LDV measurements in the down-comer verticals from Obermair et al. [7] showed that the tangential velocity in the down-comer increased by approximately 2.6 times the inlet velocity and 3.15 times in the hopper centre as opposed to the present simulation results. The reason for the difference may be due to the hopper sizes in the present tested cyclone and that by Obermair et al. [7]. The present study used a larger hopper (approximately equal to the volume of the cyclone cylindrical section), but Obermair et al. [7] tested a smaller hopper size. Therefore, the tangential velocity may increase inside the down-comer and inside the hopper centre due to the lower energy dissipation when the flow travels from the down-comer to the hopper. Inside the hopper, however, the radial reduction of the tangential velocity component towards the walls was visualized similar to the present simulation results.

The tangential velocity profiles shown in Fig. 8 for sections A-A, C-C and F-F also confirm that the tangential velocities in conventional types (Hopper 1 and Hopper 2) are the highest, approximately similar to the inlet velocity. Thus, in conventional hopper designs, the vortex continues to the hopper bottom, promoting more particle re-entrainment. Identical flow patterns were found by Qian et al. [13] for cyclone separators with and without down-comer tubes. The authors tested down-comers with the lengths of 1.5D, 2.0D and 2.5D and compared these to the conventional design. The maximum velocity found in the conventional hopper was 21 m/s, while that inside the hopper with the 2.5D height down-comer was 8 m/s [13]. The study also found that the higher tangential velocities inside conventional dust collection sections worsen the separation process by producing a re-entrainment of already separated particles.

However, higher tangential velocities inside down-comers in Fig. 8 show a dramatic increment in the quasi-free vortex, thus creating higher centrifugal forces on the particles, especially on the finer range (course particles are mostly separated in the cyclone body due to higher moments of inertia) and increased separation efficiency.

*3.1.3. Radial velocity*

The radial velocity distribution does not cover any general pattern like the tangential and axial velocity components inside the cyclone body (Fig. 9). However, the contour plots of radial velocity show that the flow is rotational and approximately symmetrical at the down-comer tube (Fig. 9 and section C-C in Fig. 10), which enhances the transport of particles into the cyclone walls. An identical flow phenomenon was observed at the cyclone conical region by Wang et al. [50]. The authors further reported that the forced-vortex region was a twisted cylinder, analysing the radial velocity distribution. However, much of the previous research [36,49] has neglected the radial velocity component, and it is therefore difficult to conclude on the radial velocity flow pattern with the literature.

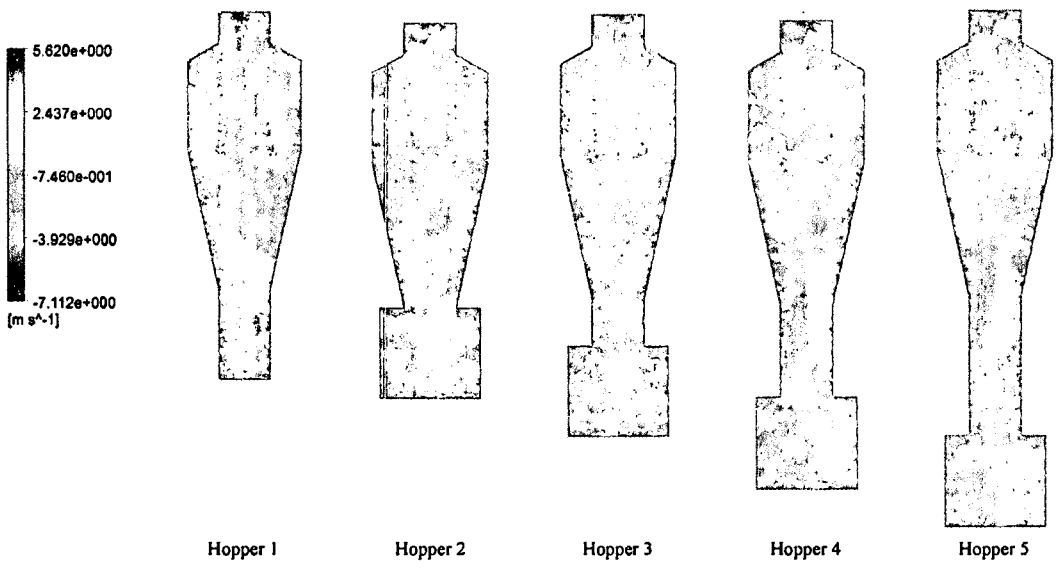


**Fig. 9.** Radial velocity contours along the vertical axis of cyclone separators with different dust outlet geometries.

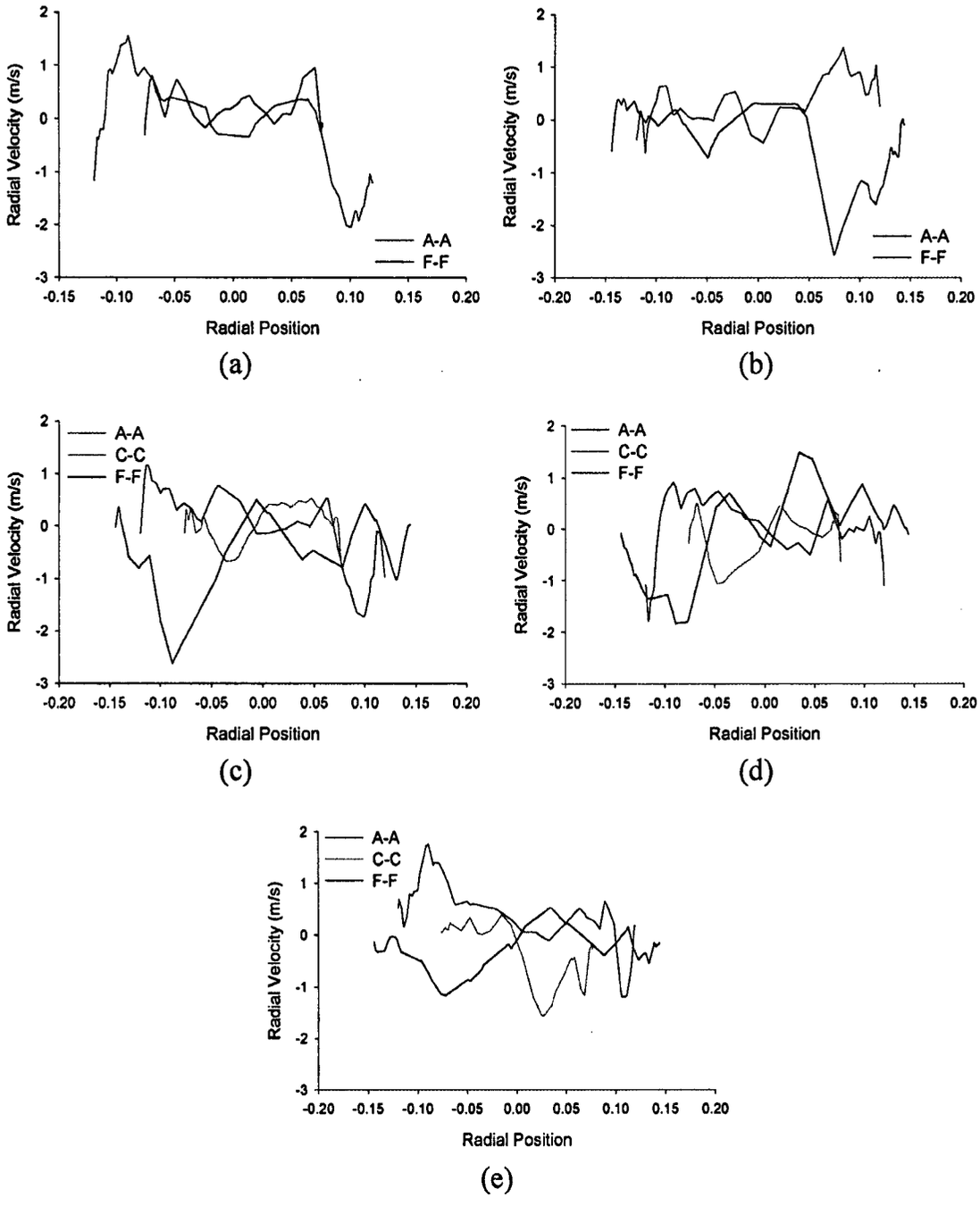


**Fig. 10.** Radial velocity components along radial direction at different cross sections in cyclone separator and dust outlet geometry (a) Hopper 1; (b) Hopper 2; (c) Hopper 3; (d) Hopper 4 and (e) Hopper 5.

The radial distributions of this velocity component for selected cross sections in Table 5 are shown in Fig. 10. Considering the radial velocity distribution in hoppers by section F-F, the non-symmetry of the distribution was visible in Hopper 2 and Hopper 3. The minimum radial velocity is observed in Hopper 1, and the maximum in Hopper 3. However, in Hopper 4 and Hopper 5, the distribution is approximately symmetric and rotational, enhancing particle separation as explained previously.

### *3.2. Pressure distribution*

#### *3.2.1. Dynamic pressure*

The contour patterns of the dynamic pressure distributions on the axial plane and horizontal planes as listed in Table 5 are shown in Figs. 11 and 12, respectively. The dynamic pressure is larger in the quasi-free vortex zone and reaches zero in the quasi-forced region in the cyclone body. A similar pattern is visible inside the down-comer tubes, and with increased height, the pressure drop reduced downward along the vertical axis. However, with the effects of non axi-symmetry of velocity, especially in the tangential velocity that dominates swirling flow, the dynamic pressure is not axi-symmetric (see Fig. 13). The maximum dynamic pressure found in the cyclone was in Hopper 4, with the effect of larger tangential velocities at the cyclone conical part.

Figs. 11 and 12 show that negative dynamic pressure zones are located at the bottom of the hoppers in Hopper 1, Hopper 2, Hopper 3 and Hopper 4 due to the reduction of velocity from the upward turning of the flow. However, considering Hopper 5, the upward turning point of the flow field is located above the hopper base, thus presenting a

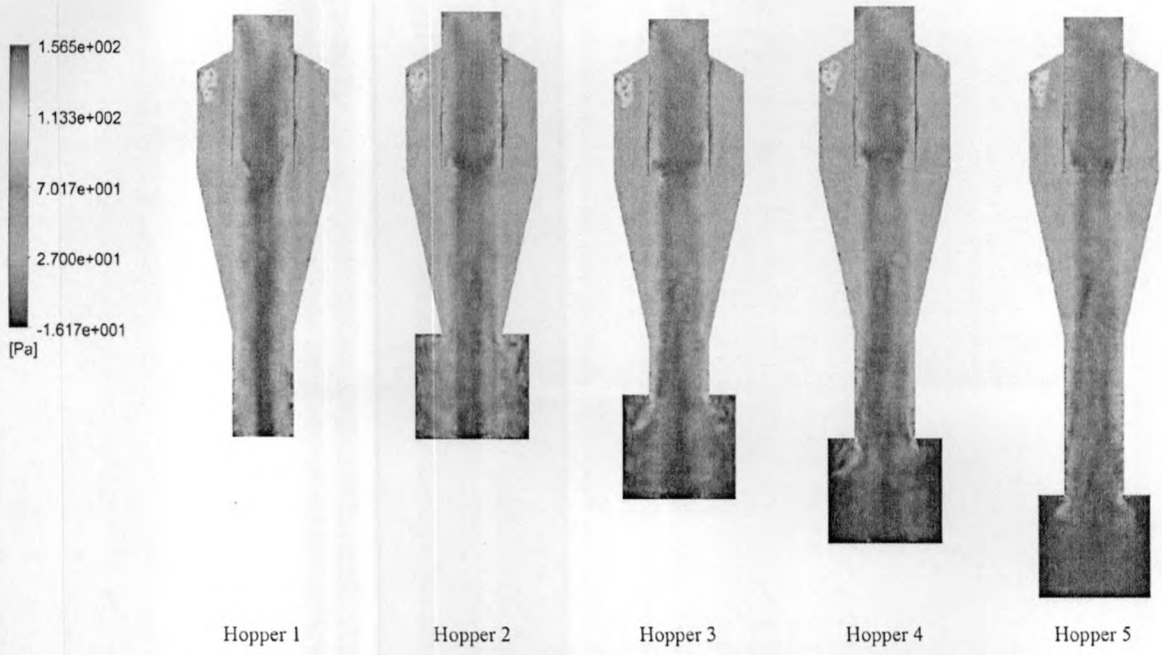


**Fig. 11.** Dynamic pressure contours along the vertical axis of cyclone separators with different dust outlet geometries.

negative pressure distribution in the Hopper 5 condition. The reduction of velocity at Hopper 5 is clearly visible in Figs. 5, 8 and 10.

Furthermore, Hopper 1 has the maximum dynamic pressure due to the highest tangential velocities, and Hopper 2 and Hopper 3 present an axi-symmetric distribution of the dynamic pressure inside the hopper across the middle plane (section F-F in Fig. 13(b) and (c)). Then, with increasing down-comer height, the dynamic pressure distribution becomes flatter inside the Hopper 4 and Hopper 5 conditions as described previously.

### 3.2.2. Static pressure

The static pressure variation is similar in all of the geometric conditions and generally non axi-symmetric (see Fig. 14). The highest static pressure zones are located in the cyclone body, *i.e.*, in the quasi-free vortex region, and the magnitude dramatically decreases from the wall to the centre axis (quasi-forced vortex region) due to the high swirling velocity. Although static pressure shows a dramatic decrease in the radial direction, the axial variation is smaller.

The maximum and minimum static pressures were found in Hopper 1 (see Figs. 14 and 15), which exhibits a lower static pressure at the cyclone bottom, showing higher turbulent flows inside. Different results were reported by Elsayed and Lacor [28] by numerical studies with the same geometries as Hopper 1 and Hopper 2. They observed that the minimum static pressure was in the cyclone with Hopper 2. Figs. 14 and 15 show that in Hopper 1 and Hopper 2, the minimum static pressure distribution is spread around the cyclone centre axis and continues into the hopper; however, in other hopper conditions, the minimum static pressure continues until the end of the down-comer tube for Hopper 3 and Hopper 4 and up to a half distance of the down-comer tube in hopper 5. The static pressure increases during its downward extension due to the higher tangential velocities inside the down-comers and the sudden contraction of the quasi-forced vortex.

Comparing the radial distribution of the static pressure in the cyclone body in the down-comer tubes and in the hoppers as shown in Fig. 16, the static pressure in the conventional cyclones in Hopper 1 and Hopper 2 contains relatively larger distributions, which are similar to the static pressure at the cyclone body (considering section A-A). With increasing down-comer length, the static pressure inside the hopper becomes lower, not because of increased turbulent kinetic energy, but by decreased total pressure (with reduced turbulence). In addition, the gradient of the static pressure in the radial direction is lower inside the hoppers with down-comers.

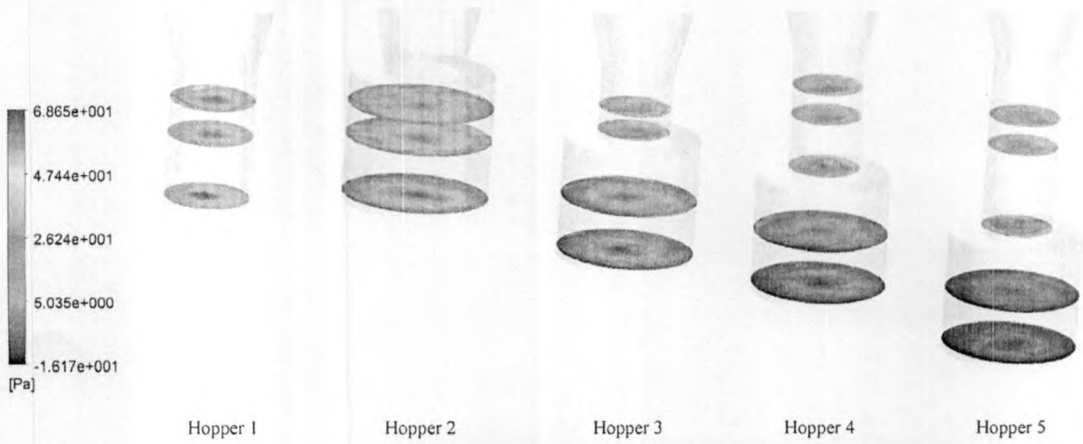


**Fig. 12.** Dynamic pressure contours on radial planes of different dust outlet geometries in cyclone separator.

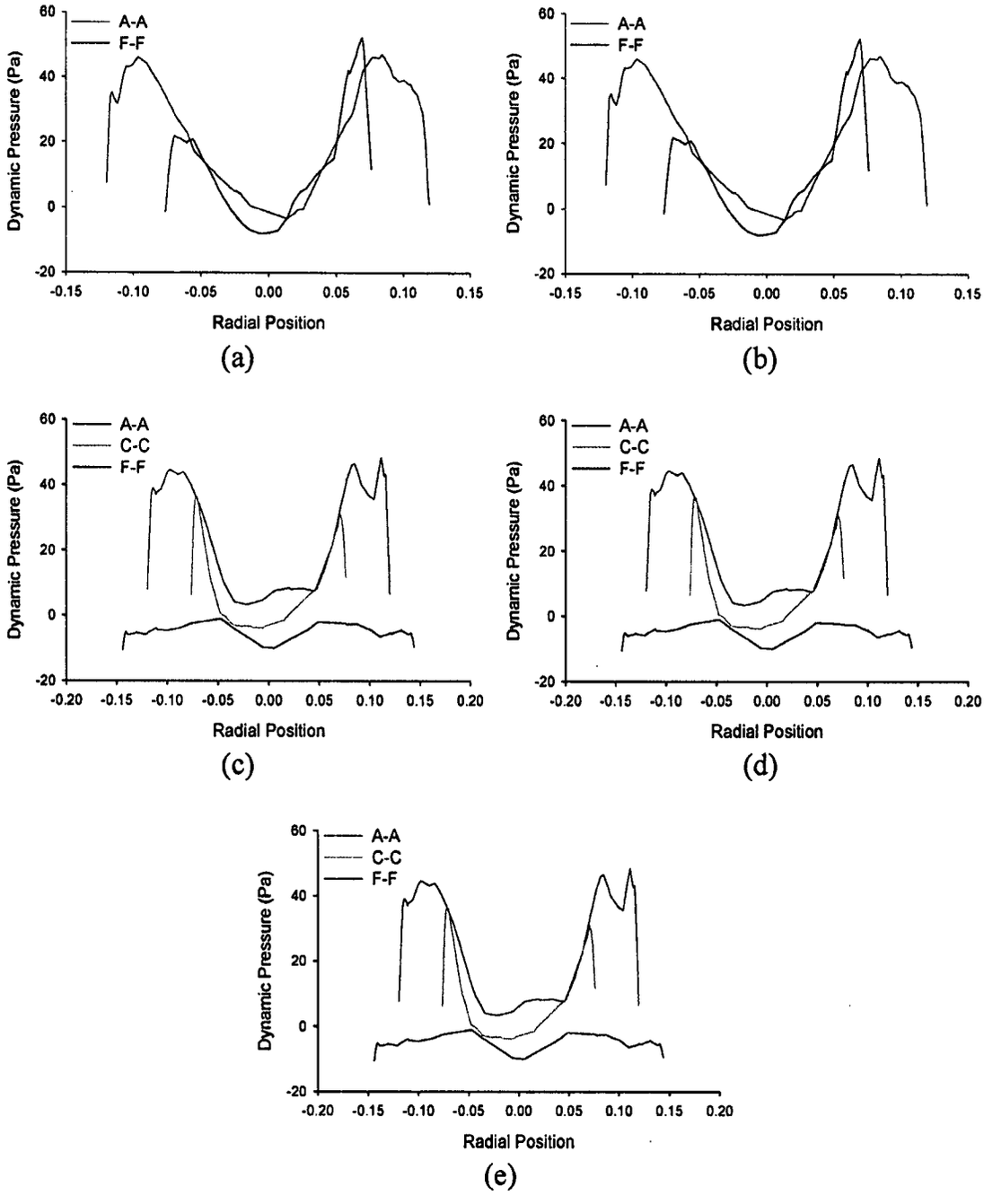


**Fig. 13.** Dynamic pressure distribution along radial direction at different cross sections in cyclone separator and dust outlet geometry (a) Hopper 1; (b) Hopper 2; (c) Hopper 3; (d) Hopper 4 and (e) Hopper 5.

### 3.3. Particle flow inside cyclone separator

Many studies [21,50,53] reported both experimentally and numerically that larger particles deposit in cyclone flow after a few strands, but smaller particles are dragged by the carrier flow. Shukla et al. [29] performed a dispersed phase model in a cyclone separator flow field and compared the centrifugal and drag forces along the particle trajectories at three different locations. They reported that the dominant force for particles larger than 2.1 μm was centrifugal force and that for particles with diameters smaller than 2.1 μm, the drag force could balance the centrifugal force. In addition, they observed that the drag force became dominant at few points along the trajectories.

However, the flow field variations inside the cyclone separators due to dust outlet geometry variations influence the particle flow paths. Thus, the probability of collection or loss is strongly affected by the dust outlet geometry. Therefore, a collected particle in one geometric condition can be lost in another geometric condition. The present study has considered particle trajectories of similar diameters relative to different dust outlet geometries. However, the injection position may change due to automatic generation of particle positions at the inlet by the software; therefore, the comparison may be limited to several hopper conditions for a considered particle, but not for all.

Three particle tracks with diameters of 0.9357, 3.5465 and 6.0423 μm were considered (Figs. 17 to 19) to analyse the trajectories of different particle diameters in cyclone gas–solid flow fields with different dust outlet geometries, which were injected from same general areas at the inlet face. These particles were selected by considering different particle fates (whether collected or lost) in five different cyclone

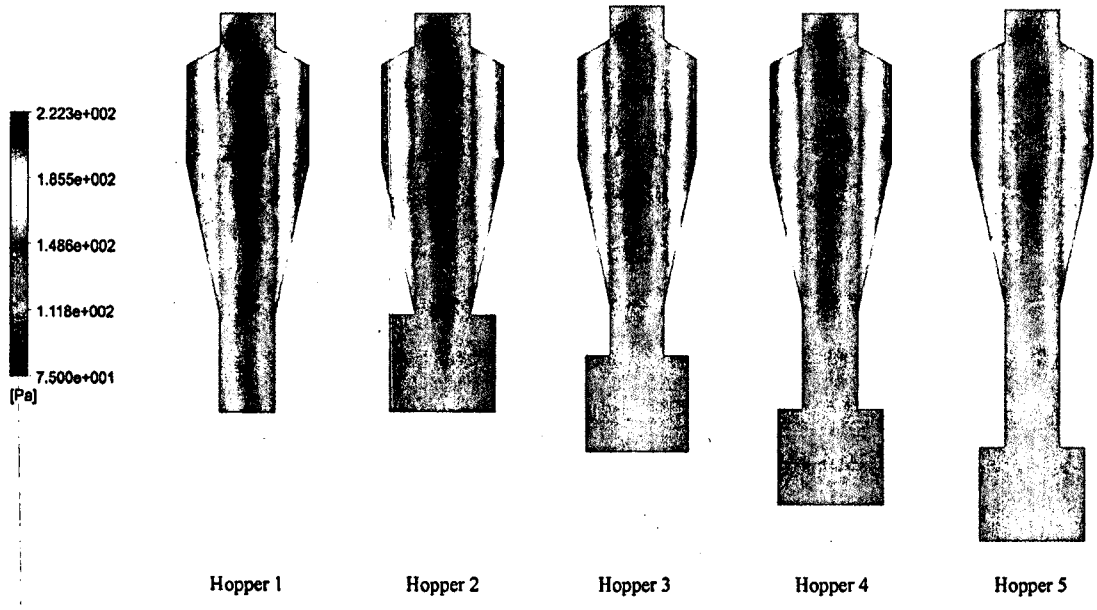


**Fig. 14.** Static pressure contours along the vertical axis of cyclone separators with different dust outlet geometries.

geometries. With the effect of different particle trajectories in different dust outlet conditions, collection or loss cannot be justified. In addition, these particle trajectories may further vary with the effect of higher concentrations and particle–particle interactions, which were not considered in the present simulations.

The smallest particle (Fig. 17) with a diameter of 0.9357 μm is lost in each hopper condition except for Hopper 4 and Hopper 5. It is well shown that the number of turns that the particle completed before exiting the cyclone was higher in Hopper 1 and Hopper 2. The particle flow in Hopper 3 is avoided here as it escaped in the secondary flow. Whirling was reduced in cyclones with down-comer tubes, which are Hopper 4 and Hopper 5. Previous researchers, such as Mothes [6] and Zhu and Lee [5], reported that the particle flow is more complex with re-entrainment of particles inside the conical part of conventional cyclone separators, especially near the cone bottom. Therefore, in Hopper 1 and Hopper 2, smaller particles follow complex paths and are mostly lost with the leaving air flow. However, due to the higher tangential flows inside down-comers, particles are easily directed into the hoppers. A similar trend is observed for the particle of 3.5465 μm diameter (Fig. 18) compared to the trajectories in Hopper 2 through Hopper 5. Particle back mixing from the quasi-forced vortex to the quasi-free vortex is also evident in Hopper 2 and Hopper 3. The larger particle with the diameter of 6.0423 μm (Fig. 19) in Hopper 2, Hopper 3 and Hopper 4, which have similar particle injection points, shows that with a larger descending angle, as in Hopper 3 and Hopper 4, the number of turns in the particle trajectory becomes low. However, Hopper 5 shows that decreasing tangential velocity along the down-comer may help particles to escape easily. One common feature in the particle trajectories is that when a particle follows the secondary flow, it has the maximum probability of escape, and if it does not escape, the particle undergoes a longer residence time (many spins) before being collected into the hopper (see the 6.0423 μm diameter particle trajectory in Hopper 1 in Fig. 19).

Furthermore, in a CFD analysis without considering the dust outlet geometry, Wang et al. [50] reported that particles entering through the upper part of a cyclone can easily exit with the flow field regardless of the particle diameter due to lower descending angles. However, the present numerical results show that the particle trajectories are strongly affected by flow field variation due to the geometry of the dust collection section. The simulation results for uncollected particle trajectories of particle sizes of 5–10 μm are shown in Fig. 20 for cyclones with Hopper 1, Hopper 2 and Hopper 5.

Fig. 20 shows that all of the un-collected particles in the cyclone with Hopper 1 are injected from the upper part of the inlet face, but in the

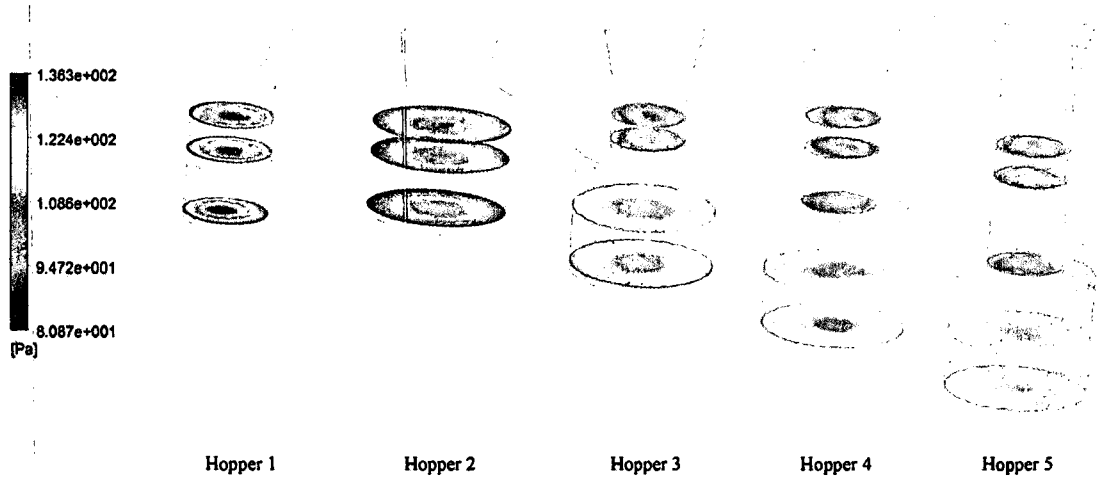


**Fig. 15.** Static pressure contours on radial planes of different dust outlet geometries in cyclone separator.

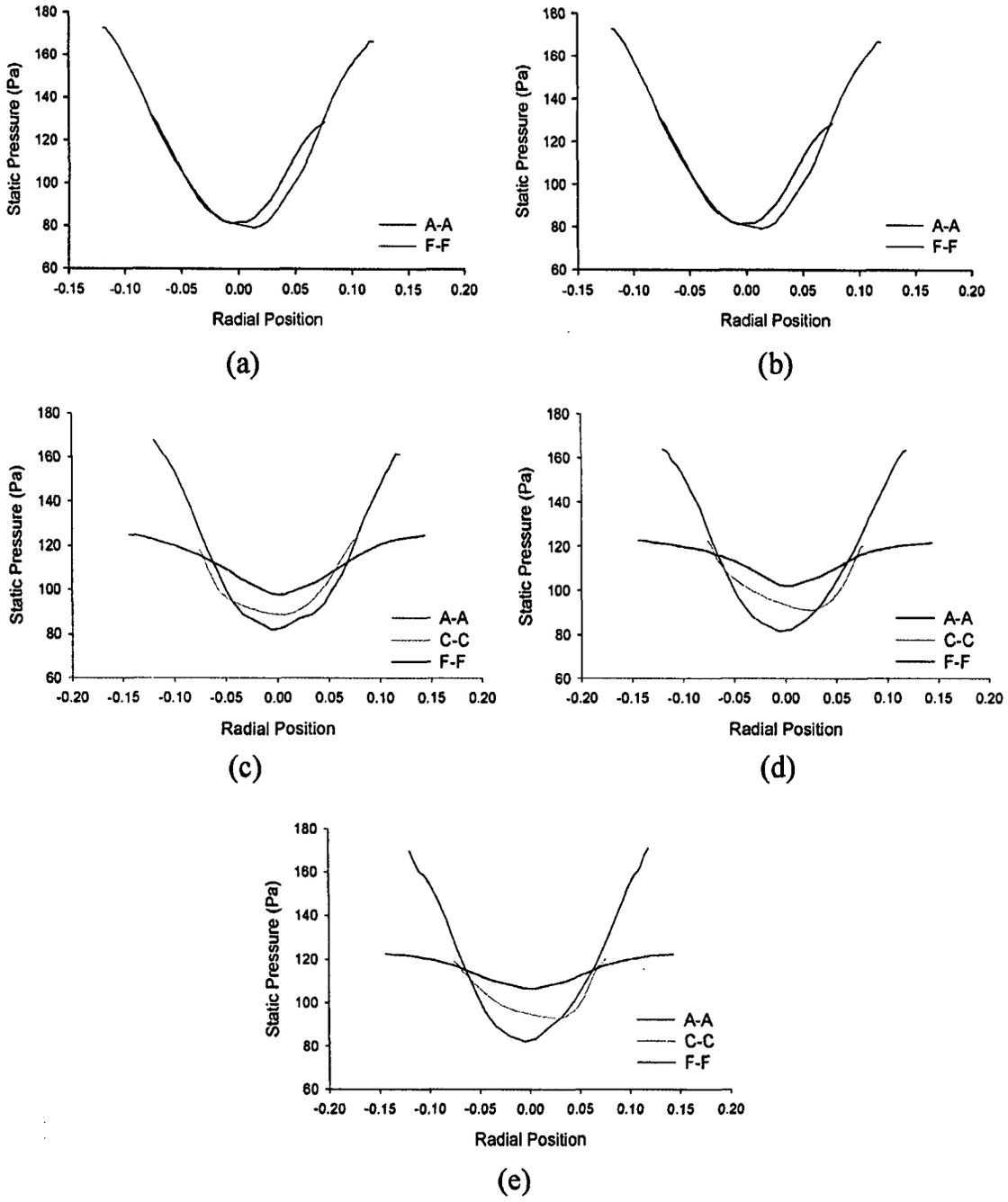


Fig. 16. Static pressure distribution along radial direction at different cross sections in cyclone separator and dust outlet geometry (a) Hopper 1; (b) Hopper 2; (c) Hopper 3; (d) Hopper 4 and (e) Hopper 5.

other four cyclones (the figures shown here are only for Hopper 2 and Hopper 3), there is no such dependence. Furthermore, comparing the uncollected 5–10 μm diameter particles in Hopper 2 and Hopper 5 conditions, the larger diameter particles that entered mostly from the inlet top have escaped in Hopper 2, while no significant correlation is shown between escaped particle size and the location in Hopper 5. Therefore, the importance of the dust collection section and its geometry in particle separation it is again verified and should be accounted for in CFD simulations.

### 3.4. Collection efficiency

Comparing the grade efficiency curves of different dust outlet geometries in Fig. 21 at the inlet solid loading rate of 1.0 g/m$^3$, Hopper 1 has the maximum separation and Hopper 2 has the lowest. Both Hopper 4 and Hopper 5 conditions have similar grade efficiency curves, while Hopper 3 has poorer grade efficiency in the 0.5–1.99 μm diameter fraction and follows Hopper 4 and Hopper 3 for other particle fractions.

The grade efficiency curve comparisons to the experimental grade efficiencies are shown in Fig. 22 to validate the numerical results.

The numerical grade efficiencies were modified before comparison according to the particle diameter fractions in the experiments. Comparing the numerical grade efficiency curves with different X-axes (log based and fractional based) shown in Figs. 21 and 22 gives similar general trends.

Fig. 22 shows that the numerical grade efficiency curves are different from the experimental grade efficiency curves and that the deviation

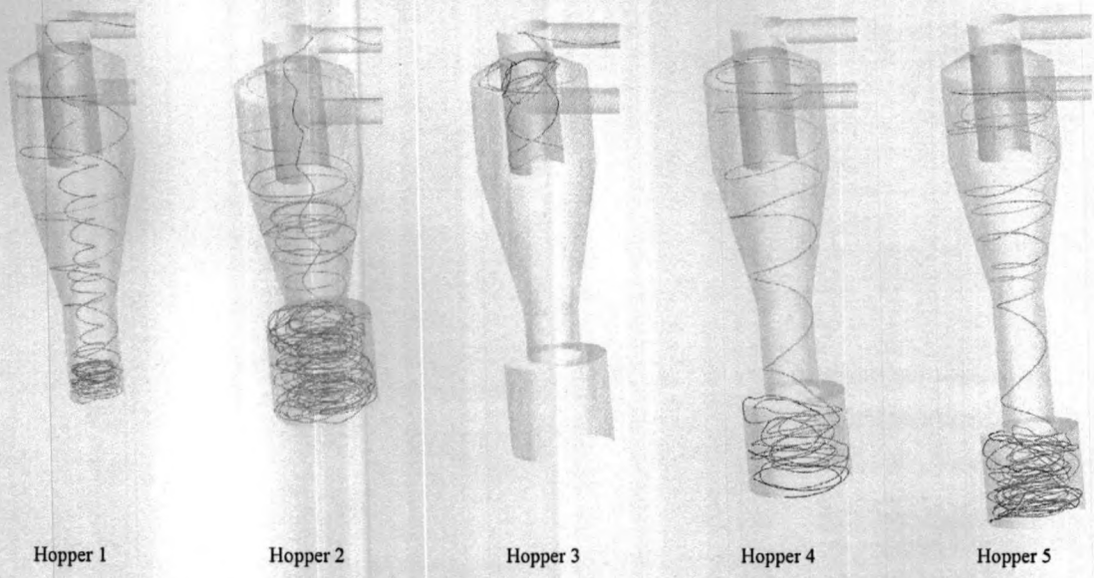


**Fig. 17.** Particle trajectory of 0.9357 μm particle inside cyclone separators with different dust outlet sections.

between the results are higher for particle fractions smaller than 2.0 μm for all cases excluding Hopper 1. For particles larger than 2.0 μm diameter, the numerical results of cyclones with down-comer tubes are closer to the experimental investigations with maximum deviation of 13.34 % in Hopper 3 for the 5.0–9.99 μm size range.

Analysing the numerical and experimental grade efficiency curves for Hopper 1, although it had the lowest grade efficiency level among other dust outlet geometries from the experiments, it was the highest in numerical simulations. This result is due to the particle fate criterion of collection at the hopper bottom. In CFD modelling, due to the small diameter and smaller height of Hopper 1, the entered particles can easily touch the hopper bottom of the cyclone with higher tangential velocity and be collected due to the lack of considering particle back mixing, which is found in practice. Hopper 2 shows the minimum collection efficiency for particles lower than 2.0 μm, when comparing the grade efficiency curves (Fig. 21). Having a larger hopper, smaller particle trajectories entering to the hopper may follow larger diameter curvy paths, hence reducing velocity and back-mixing. The tangential velocity distributions for Hopper 1 and Hopper 2 in Figs. 6 and 7 also verify this difference. For the particles larger than 5 μm, Hopper 2 over estimates the grade efficiencies over the experiments due to the particle re-entrainment in practice.

In summary, apart from Hopper 1, the numerical grade efficiency always under predicted the collection efficiencies for smaller particles (<2.0 μm) for all dust collection sections. The reason for under prediction of the fine particle ranges is due to particle agglomeration with larger particles and separation, which has been investigated by many previous studies [11,12,39,54–57]. However, it is difficult to account for particle agglomeration numerically due to the lack of information about particle separation.

Even though particle collection efficiencies for the range of less than 2.0 μm are under predicted by Hopper 3, Hopper 4 and Hopper 5, the grade efficiencies are higher than Hopper 2, which consists of a conventional type dust outlet systems. Thus, particle re-entrainment can be

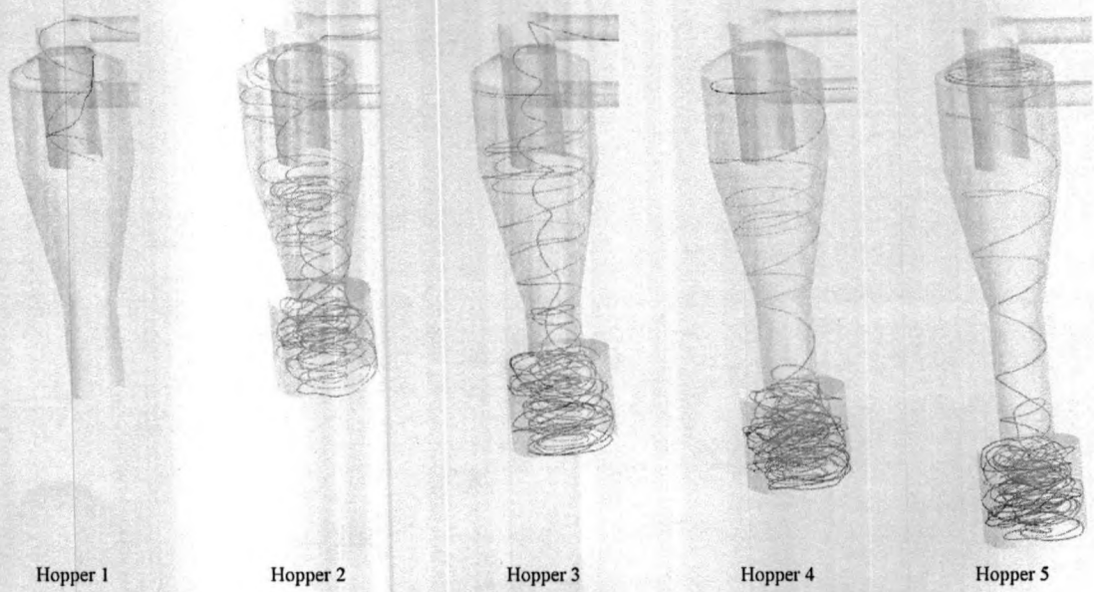


**Fig. 18.** Particle trajectory of 3.5465 μm particle inside cyclone separators with different dust outlet sections.

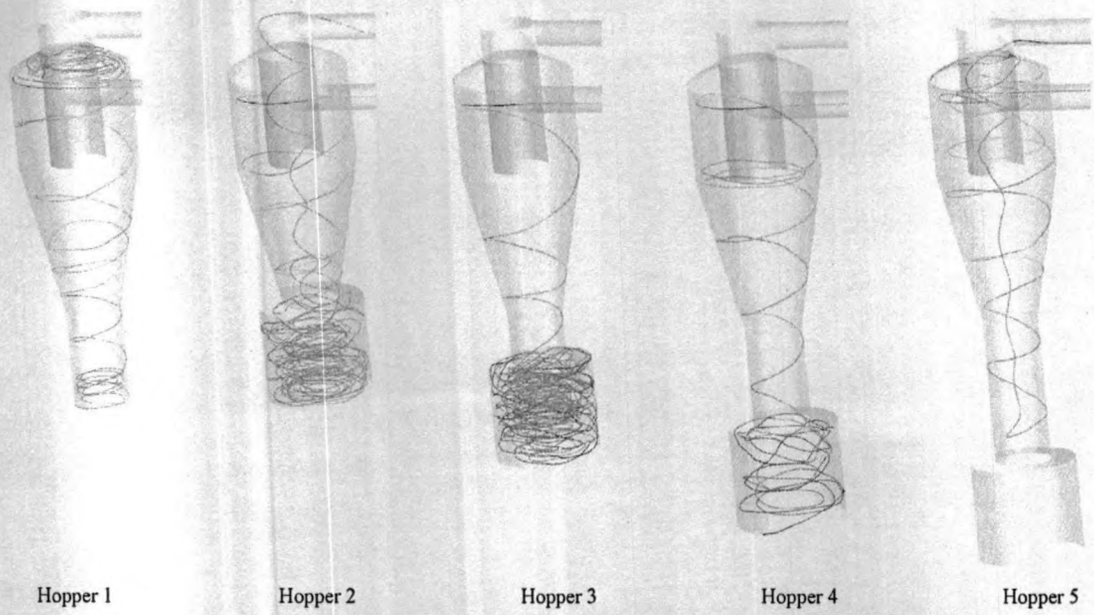


**Fig. 19.** Particle trajectory of 6.0423 μm particle inside cyclone separators with different dust outlet sections.

minimized with the application of down-comer tubes, which is proven by experiments in the present study. Similar collection efficiency enhancement by the application of down-comers has been reported by Obermair and Staudinger [8] by experiments.

To calculate the overall collection efficiency, number based calculations were not applicable to the experimental data, which were obtained by weight. Therefore, the overall collection efficiencies from CFD simulation were calculated based on average masses of particle fractions. The comparison of the numerical and experimental overall collection efficiencies are given in Table 6.

Compared to the experimental results, the CFD simulations under predict the overall collection efficiencies for the hopper conditions with down-comer tubes. As specified previously, the overall collection efficiency is over predicted by the Hopper 1 condition, and for Hopper 2, the experimental and numerical results agreed well. The difference in the overall collection efficiencies in hoppers with down-comer tubes is due to particle agglomeration in real situations, which are not considered in simulations.

### 3.5. Pressure drop

To analyse the cyclone performance, the pressure drop is an important factor that directly relates to the operational cost of the cyclone separator. Pressure drop is mainly due to losses at the inlet, fluid swirling losses and losses in the vortex finder and exit duct and depends on wall friction, solid concentration and the geometry of the cyclone separator. Therefore, optimizing the pressure drop in cyclone separators is an important issue. The numerically and experimentally calculated pressure drops at each dust outlet condition are shown in Table 7.

In general, CFD results for pressure drops are larger than the experimental values due to the effect of particles in flow in experiments and neglecting particle influence in the continuous phase in numerical simulations by one-way coupling. Studies reported in the literature [11,28, 58–60] also showed reductions of pressure drop in cyclone separators

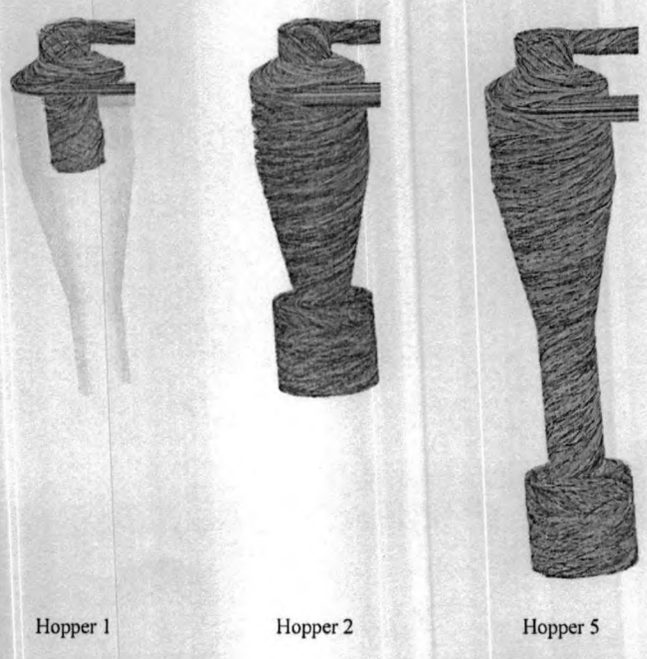


**Fig. 20.** Uncollected particle trajectories in the range of 5–10 μm in cyclone separator with different dust outlet geometries.

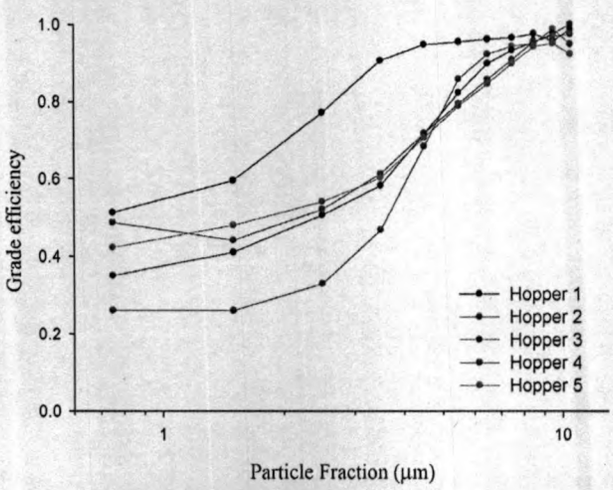


**Fig. 21.** Grade efficiency curves of particle fractions in cyclones with different dust outlet sections.

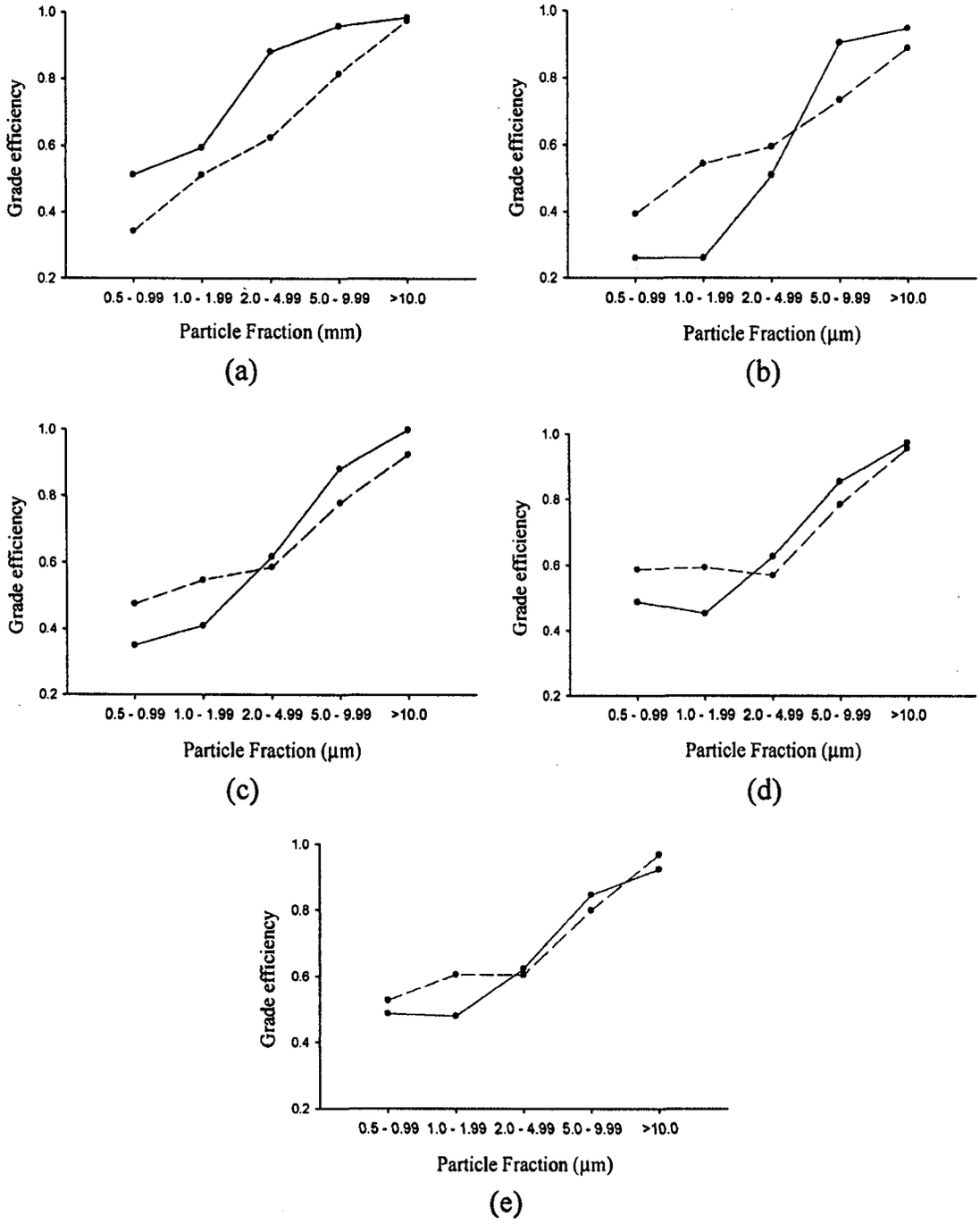


**Fig. 22.** Grade efficiency curves of particle fractions in cyclones with different dust outlet sections (a) Hopper 1; (b) Hopper 2; (c) Hopper 3; (d) Hopper 4 and (e) Hopper 5 (CFD results – straight lines, experimental results – dash lines).

**Table 6**
Overall collection efficiencies in each cyclone geometry compared with experimental and CFD results.

| Hopper condition | Overall collection efficiency | |
|---|---|---|
| | CFD | Experimental |
| Hopper 1 | 0.9571 | 0.8847 |
| Hopper 2 | 0.8735 | 0.8711 |
| Hopper 3 | 0.8561 | 0.9292 |
| Hopper 4 | 0.8433 | 0.9263 |
| Hopper 5 | 0.8725 | 0.9198 |

**Table 7**
Pressure drop in each cyclone geometry compared with experimental and CFD results.

| Hopper condition | Pressure drop (Pa) | |
|---|---|---|
| | CFD | Experimental |
| Hopper 1 | 198.74 | 157.05 |
| Hopper 2 | 202.06 | 148.73 |
| Hopper 3 | 183.83 | 150.17 |
| Hopper 4 | 206.81 | 165.37 |
| Hopper 5 | 193.24 | 168.25 |

due to the presence of particles caused by the reduction of turbulent kinetic energy [36,61,62], although higher solid loading conditions improve the wall frictional effect.

Comparing Hopper 1 and Hopper 2, the former shows a higher pressure drop in experimental investigations, but the results are inverse in the numerical investigations. Considering the factors affecting pressure drop in these two conditions, high tangential velocities in Hopper 1 contribute to dissipating kinetic energy, and there is a sudden extraction in Hopper 2 influence to reduce the pressure drop. However, considering the numerical results energy dissipation by sudden extraction of the flow field may be less significant than the higher swirl in the hopper. Considering the experimental pressure drop, the significance of the effect from the particle phase on the pressure drop shows greater pressure drop reduction in Hopper 1 than Hopper 2. Again, higher particle concentrations at the cone bottom of Hopper 2 significantly weaken the turbulent effect, and thus the effect of sudden extraction is weakened. Therefore, Hopper 2 represents a lower pressure drop than Hopper 1 in the experimental studies.

Referring to the pressure drop of cyclone separators with down-comer tubes, this modification leads to increased pressure drops compared to conventional dust outlet geometries [7,8] by increasing the wall surface area and the turbulent kinetic energy of the air flow caused by reducing solid re-entrainment. However, pressure drop values from numerical modelling shows increased pressure drop from Hopper 3 to Hopper 4 due to increase in tangential velocity inside the down-comer. Reducing the tangential velocity along the down-comer tube reduced the pressure drop in Hopper 5 more than in Hopper 4 (see Fig. 6).

The smallest pressure drop from numerical simulations was in Hopper 3, although in the experiments, it was in Hopper 2. The reason for the lower pressure drop in Hopper 3 in CFD analysis is the relatively similar energy loss and gain in sudden extraction and contraction at the cyclone bottom. However, in Hopper 4 and Hopper 5, the down-comer tubes may increase the turbulent kinetic energy and reduce this energy downward along the tubes, reducing the effect of energy loss by expansion.

In summary, considering down-comer tubes at the cyclone bottom, the pressure drop increases with down-comer length. Comparing the experimental results, the effect of particles in the flow field and separation efficiency increment due to down-comers may change the pressure drop results in numerical modelling.

## 4. Conclusions

LES based CFD modelling of cyclone separator gas–solid flow was conducted for five cyclone geometries with different dust outlet geometries to analyse the flow field and cyclone performance with down-comer tubes at the cyclone bottom. The cyclone performance parameters, collection efficiency and pressure drop were compared to the experimental results. The following conclusions were reached.

01. Higher axial and tangential velocities in conventional dust outlet geometries may worsen the collection efficiency by allowing particle re-entrainment. Conversely, cyclones with down-comer tubes before the hopper increase the magnitude of the tangential velocities inside the tube that centrifuge particles in the quasi-forced vortex to the wall and mix with the downward flow, enhancing the particle collection. The magnitude of the tangential velocity falls towards the hopper, thus minimizing particle back mixing. This effect may increase particle collection efficiency.
02. Considering the flow pattern and particle trajectories inside the cyclone separator with respect to dust outlet geometry, the dust outlet geometry may change the flow pattern and particle trajectories. Therefore, particle collection may also vary. Thus, accounting for dust outlet geometry in numerical modelling is important, although it is ignored by many simulation studies. However, many studies that have not considered the effect of dust outlets have given numerical results agreeing with experimental results as they have considered different particle collection zones. Therefore, this is still an open question.
03. Comparing simulated collection efficiencies to experimental observations, particle fractions lower than 2 μm are always under predicted numerically due to neglecting particle agglomeration, showing the importance of particle fate criteria in simulations to achieve better simulation results.
04. The difference between experimental and CFD results for pressure drops are due to the effect of particle phase in practice (turbulence reduction, particle agglomeration and increased wall friction) that are not considered in modelling.

In summary, dust collection geometries modified with down-comer tubes can increase the separation efficiency at considerable pressure drop conditions. However, the performance is strongly influenced by particle concentration in the flow field. Thus, further detailed analysis is required to optimize the cyclone efficiency with down-comer tubes.

*Nomenclature*

| | |
|---|---|
| $a$ | cyclone inlet height, m |
| $B$ | diameter of the cyclone bottom, diameter of the down-comer tube, m |
| $b$ | cyclone inlet width, m |
| $C$, $C_k$ | constant of order one in the Kolmogorov's energy cascade theory |
| $C_D$ | drag coefficient |
| $C_s$ | Smagorinsky constant |
| $D$ | diameter of cyclone body, m |
| $D_e$ | diameter of vortex finder, m |
| $D_h$ | diameter of the hopper, m |
| $d$ | diameter, μm |
| $D_i$, $D_o$ | inlet and outlet diameters of the tested cyclone separator, m |
| $E(k)$ | energy spectrum function |
| $G$ | filtering function |
| $g$ | gravitational acceleration, m/s$^2$ |
| $H$ | height of cyclone separator, $m$ |
| $H_h$ | height of the hopper, m |
| $H_t$ | height of the down-comer tube, m |
| $h$ | cyclone cylinder height, m |
| $k$ | wave length, m |
| $l$ | length scale, m |
| $P$, $p$ | pressure, Pa |
| $Q$ | flow rate, m$^3$/s |
| $q_{SGS}$ | SGS velocity scale |
| $R_e$ | Reynolds number |
| $S$ | height of vortex finder, m |
| $\overline{S}$ | large scale strain rate tensor |
| $t$ | time, s |
| $v'$ | fluctuating velocity, m/s |
| $v$ | gas velocity, instantaneous velocity, m/s |
| $v_{SGS}$ | SGS turbulent viscosity, m/s |

*Greek Letters*

| | |
|---|---|
| $\overline{\varphi}_i'$ | resolvable scale part Subgrid scale |
| $\overline{\varphi}_i$ | basic filtered variable Subgrid scale |
| $\overline{\varphi}$ | resolvable scale part |
| $\varphi_i$ | any variable at Subgrid scale |
| $\Delta$ | filter width (or grid size) |
| $\delta$ | Kronecker delta |
| $\mu$ | dynamic viscosity of air, m$^2$/s |
| $\nu$ | kinematic viscosity of the fluid, kg/ms |
| $\xi$ | $= b/R$ |

$\rho$ density, kg/m$^3$
$\tau$ shear stress components ($\tau_{ij}$)
$\epsilon$ energy dissipation rate, m$^2$/s$^3$

*Subscripts*
$e$ vortex finder, cyclone core
$g$ gas/air
$i, j, k$ $i, j$ and $k^{th}$ directions
$p, x$ particle

## Acknowledgement

The research is supported by the University Grant Committee of HKSAR grant number GRF 115712.

## References

[1] K. Lim, et al., Characteristics of the collection efficiency for a cyclone with different vortex finder shapes, J. Aerosol Sci. 35 (2004) 743–754.
[2] W.L. Heumann, Industrial Air Pollution Control Systems, vol. 620, McGraw-Hill, New York, 1997.
[3] H. Bryant, et al., How dust in gas affects cyclone pressure drop, Hydrocarb. Process. (U. S.) 62 (1983).
[4] R. Xiang, et al., Effects of cone dimension on cyclone performance, J. Aerosol Sci. 32 (2001) 549–561.
[5] Y. Zhu, K. Lee, Experimental study on small cyclones operating at high flowrates, J. Aerosol Sci. 30 (1999) 1303–1315.
[6] H. Mothes, Bewegung und Abscheidung der Partikeln im Zyklon(PhD. Thesis) Technical University Karlsruhe, Germany, 1982.
[7] S. Obermair, et al., Investigation of the flow pattern in different dust outlet geometries of a gas cyclone by laser Doppler anemometry, Powder Technol. 138 (2003) 239–251.
[8] S. Obermair, G. Staudinger, The dust outlet of a gas cyclone and its effects on separation efficiency, Chem. Eng. Technol. 24 (2001) 1259–1263.
[9] A.C. Hoffmann, et al., Evidence of the 'natural vortex length' and its effect on the separation efficiency of gas cyclones, Filtr. Sep. 32 (1995) 799–804.
[10] H.J. Kecke, Beitrag zur Klärung des Stromungsvorganges und der Staub Bewegung im Gaszyklon(PhD. theses) Technical University Magdeburg, Germany, 1967.
[11] A. Gil, et al., Effect of the solid loading on a PFBC cyclone with pneumatic extraction of solids, Chem. Eng. Technol. 25 (2002) 407–415.
[12] A.C. Hoffmann, et al., The effect of the dust collection system on the flow pattern and separation efficiency of a gas cyclone, Can. J. Chem. Eng. 74 (1996) 464–470.
[13] F. Qian, et al., Effects of the prolonged vertical tube on the separation performance of a cyclone, J. Hazard. Mater. 136 (2006) 822–829.
[14] F. Kaya, I. Karagoz, Numerical investigation of performance characteristics of a cyclone prolonged with a dipleg, Chem. Eng. J. 151 (2009) 39–45.
[15] ANSYS, ANSYS CFX14.0, Solver Modeling Documentation, ANSYS, Inc., 2011
[16] ANSYS, ANSYS CFX14.0, Solver Theory Documentation, ANSYS, Inc., 2011
[17] C. Rhie, W. Chow, Numerical study of the turbulent flow past an airfoil with trailing edge separation, AIAA J. 21 (1983) 1525–1532.
[18] A. Kępa, Division of outlet flow in a cyclone vortex finder—the CFD calculations, Sep. Purif. Technol. 75 (2010) 127–131.
[19] G. Wan, et al., Solids concentration simulation of different size particles in a cyclone separator, Powder Technol. 183 (2008) 94–104.
[20] Y. Qiu, et al., Numerical study of the flow field and separation efficiency of a divergent cyclone, Powder Technol. 217 (2012) 231–237.
[21] L. Ma, et al., Numerical modelling of the fluid and particle penetration through small sampling cyclones, J. Aerosol Sci. 31 (2000) 1097–1119.
[22] W. Griffiths, F. Boysan, Computational fluid dynamics (CFD) and empirical modelling of the performance of a number of cyclone samplers, J. Aerosol Sci. 27 (1996) 281–304.
[23] H. Yoshida, et al., Effect of apex cone height on particle classification performance of a cyclone separator, Adv. Powder Technol. 14 (2003) 263–278.
[24] J. Gimbun, et al., Prediction of the effects of cone tip diameter on the cyclone performance, J. Aerosol Sci. 36 (2005) 1056–1065.
[25] T. Chuah, et al., A CFD study of the effect of cone dimensions on sampling aerocyclones performance and hydrodynamics, Powder Technol. 162 (2006) 126–132.
[26] K.U. Bhaskar, et al., CFD simulation and experimental validation studies on hydrocyclone, Miner. Eng. 20 (2007) 60–71.
[27] K. Elsayed, C. Lacor, Numerical modeling of the flow field and performance in cyclones of different cone-tip diameters, Comput. Fluids 51 (2011) 48–59.
[28] K. Elsayed, C. Lacor, The effect of the dust outlet geometry on the performance and hydrodynamics of gas cyclones, Comput. Fluids 68 (2012) 134–147.
[29] S.K. Shukla, et al., Evaluation of numerical schemes for dispersed phase modeling of cyclone separators, Eng. Appl. Comput. Fluid Mech. 5 (2011) 235–246.
[30] L. Shi, D.J. Bayless, Comparison of boundary conditions for predicting the collection efficiency of cyclones, Powder Technol. 173 (2007) 29–37.
[31] M. Bohnet, Influence of the gas temperature on the separation efficiency of aerocyclones, Chem. Eng. Process. Process Intensif. 34 (1995) 151–156.
[32] K. Lim, et al., An experimental study of the performance factors affecting particle collection efficiency of the electrocyclone, Aerosol Sci. Technol. 35 (2001) 969–977.
[33] H. Yoshida, et al., Particle separation by Iinoya's type gas cyclone, Powder Technol. 118 (2001) 16–23.
[34] F.J. de Souza, et al., Large eddy simulation of the gas–particle flow in cyclone separators, Sep. Purif. Technol. 94 (2012) 61–70.
[35] J. Derksen, Separation performance predictions of a Stairmand high efficiency cyclone, AIChE J 49 (2003) 1359–1371.
[36] J. Derksen, et al., Simulation of mass-loading effects in gas–solid cyclone separators, Powder Technol. 163 (2006) 59–68.
[37] S. Schmidt, et al., Simulation of turbulent flow in a cyclonic separator, Third International Conference on CFD in the Minerals and Process Industries, Melbourne, Australia 2003, pp. 365–369.
[38] M. Slack, et al., Advances in cyclone modelling using unstructured grids, Chem. Eng. Res. Des. 78 (2000) 1098–1104.
[39] E. Hugi, L. Reh, Focus on solids strand formation improves separation performance of highly loaded circulating fluidized bed recycle cyclones, Chem. Eng. Process. Process Intensif. 39 (2000) 263–273.
[40] J. Derksen, H. Van den Akker, Simulation of vortex core precession in a reverse-flow cyclone, AIChE J 46 (2000) 1317–1331.
[41] W. Martignoni, et al., Evaluation of cyclone geometry and its influence on performance parameters by computational fluid dynamics (CFD), Braz. J. Chem. Eng. 24 (2007) 83–94.
[42] H. Shalaby, et al., Comparative study of the continuous phase flow in a cyclone separator using different turbulence models, Int. J. Numer. Methods Fluids 48 (2005) 1175–1197.
[43] H. Shalaby, et al., Particle-laden flow simulation in a cyclone separator, PAMM 6 (2006) 547–548.
[44] J.R. Schwab, Turbulence modeling, in: V.K. Garg (Ed.), Applied Computational Fluid Dynamics, CRC Press 1998, pp. 81–93.
[45] J. Smagorinsky, General circulation experiments with the primitive equations: I. The basic experiment*, Mon. Weather Rev. 91 (1963) 99–164.
[46] S. Lain, Study of turbulent two-phase gas–solid flow in horizontal channels, Indian J. Chem. Technol. 20 (2013) 128–136.
[47] C. Cortes, A. Gil, Modeling the gas and particle flow inside cyclone separators, Prog. Energy Combust. Sci. 33 (2007) 409–452.
[48] S. Elghobashi, On predicting particle-laden turbulent flows, Appl. Sci. Res. 52 (06/01/1994) 309–329.
[49] W. Peng, et al., Flow pattern in reverse-flow centrifugal separators, Powder Technol. 127 (2002) 212–222.
[50] B. Wang, et al., Numerical study of gas–solid flow in a cyclone separator, Appl. Math. Model. 30 (2006) 1326–1342.
[51] R. Utikar, et al., Hydrodynamic Simulation of Cyclone Separators, 2010.
[52] A. Hoekstra, et al., An experimental and numerical study of turbulent swirling flow in gas cyclones, Chem. Eng. Sci. 54 (1999) 2055–2065.
[53] E. Muschelknautz, V. Greif, Cyclones and other gas–solids separators, Circulating Fluidized Beds, Springer 1997, pp. 181–213.
[54] T. Chan, M. Lippmann, Particle collection efficiencies of air sampling cyclones: an empirical theory, Environ. Sci. Technol. 11 (1977) 377–382.
[55] V.G. Chibante, et al., Comparing the performance of recirculating cyclones applied to the dry scrubbing of gaseous HCl with hydrated lime, Ind. Eng. Chem. Res. 48 (2008) 1029–1035.
[56] R.L. Salcedo, Collection efficiencies and particle size distributions from sampling cyclones — comparison of recent theories with experimental data, Can. J. Chem. Eng. 71 (1993) 20–27.
[57] R.L. Salcedo, M.J. Pinho, Pilot-and industrial-scale experimental investigation of numerically optimized cyclones, Ind. Eng. Chem. Res. 42 (2003) 145–154.
[58] F.L. Fassani, L. Goldstein Jr., A study of the effect of high inlet solids loading on a cyclone separator pressure drop and collection efficiency, Powder Technol. 107 (2000) 60–65.
[59] A.C. Hoffmann, et al., Effects of geometry and solid loading on the performance of gas cyclones, Powder Technol. 70 (1992) 83–91.
[60] S. Yuu, et al., The reduction of pressure drop due to dust loading in a conventional cyclone, Chem. Eng. Sci. 33 (1978) 1573–1580.
[61] F. Qian, et al., Numerical study of the separation characteristics in a cyclone of different inlet particle concentrations, Comput. Chem. Eng. 31 (2007) 1111–1122.
[62] X. Xue, et al., Numerical simulation of particle concentration in a gas cyclone separator, Pet. Sci. 4 (2007) 76–83.